Icarus 232 (2014) 118–132

Contents lists available at ScienceDirect

Icarus

journal homepage: www.elsevier.com/locate/icarus

Planetesimal-driven migration of terrestrial planet embryos ☆

David A. Minton [a,*], Harold F. Levison [b]

[a] Purdue University, Department of Earth, Atmospheric, & Planetary Sciences, 550 Stadium Mall Drive, West Lafayette, IN 47907, United States
[b] Southwest Research Institute and NASA Lunar Science Institute, 1050 Walnut St. Suite 300, Boulder, CO 80302, United States

ARTICLE INFO

Article history:
Received 7 February 2012
Revised 23 December 2013
Accepted 1 January 2014
Available online 13 January 2014

Keywords:
Origin, Solar System
Planetary formation
Planetesimals

ABSTRACT

We develop a model for planetesimal-driven migration (PDM) in the context of rocky planetary embryos in the terrestrial planet region during the runaway and oligarchic growth phases of inner planet formation. We develop this model by first showing that there are five necessary and sufficient criteria that must be simultaneously satisfied in order for a rocky inner Solar System embryo to migrate via PDM. To investigate which embryos within a given disk satisfy the five criteria, we have developed a Monte Carlo planetesimal merger code that simulates the growth of embryos from a planetesimal disk with nebular gas. The results of our Monte Carlo planetesimal merger code suggest that, for typical values of the minimum mass solar nebula for the inner Solar System, an average of 0.2 embryos capable of PDM emerge over the lifetime of the disk. Many disks in our simulations produce no migration candidates, but some produced as many as 3. The number of embryos that experience PDM in a disk increases with increasing disk mass and decreasing il planetesimal mass, although we were not able to simulate disks where the average initial planetesimal size was smaller than 50 km. For disks 4× more massive than the standard minimum mass solar nebula, we estimate that an average of 1.5 embryos capable of PDM emerge, with some producing as many as 7.

© 2014 The Authors. Published by Elsevier Inc. All rights reserved.

1. Introduction

A phenomenon called planetesimal-driven migration (PDM) has been studied in the context of the evolution of giant planet orbits (Fernandez and Ip, 1984; Malhotra, 1993; Levison et al., 2007) and giant planet cores (Levison et al., 2010). PDM arises from the asymmetric scattering by a large body embedded in a disk of planetesimals (Kirsh et al., 2009). When a large body preferentially scatters planetesimals either inward (toward the Sun) or outward (away from the Sun), net orbital angular momentum is transferred between the disk and the large body, causing a drift in the large body's semimajor axis. Simulations of rocky planet formation in the inner Solar System have not included PDM, because, as we will show, these simulations have not had the resolution necessary to resolve this process.

Unfortunately, as we discuss in more detail below, we cannot yet perform a single end-to-end calculation of terrestrial planet formation that captures the important physical processes accurately enough. We designed a multi-stepped series of calculations that are intended to focus on evaluating whether PDM should be considered an important process in terrestrial planet formation, rather than to perform accurate terrestrial planet formation simulations. In particular, our goal is to determine the conditions that lead to PDM of terrestrial embryos, and show how the growth history of embryos is altered for those objects that undergo PDM.

Using N-body simulations, we identify five criteria that must be simultaneously met in order for PDM to take place, which are each described in detail in Section 2.3. In Section 3 we use a newly developed Monte Carlo code called *GAME* (Growth And Migration of Embryos) to model planetary accretion through the runaway and oligarchic regimes. We use results of *GAME*, coupled with our migration criteria, to show when and where PDM can occur for a variety of plausible models for the inner Solar System planetesimal disk. As we will show in more detail, PDM allows a small number of embryos to become highly mobile in the disk. This mobility may alter the assumption about how embryos and planetesimals are distributed in the terrestrial planet disk during the start of late-stage accretion.

1.1. Summary of planet formation models

We briefly summarize the "standard" methods used to study the formation of terrestrial planets in order to understand why PDM has not been seen in previous work. The bodies of the inner Solar System are thought to have formed in a hierarchical process that began with dust grains entrained within a gaseous disk and

☆ This is an open-access article distributed under the terms of the Creative Commons Attribution-NonCommercial-No Derivative Works License, which permits non-commercial use, distribution, and reproduction in any medium, provided the original author and source are credited.

* Corresponding author.
E-mail address: daminton@purdue.edu (D.A. Minton).

0019-1035/$ - see front matter © 2014 The Authors. Published by Elsevier Inc. All rights reserved.
http://dx.doi.org/10.1016/j.icarus.2014.01.001

ended with Mercury, Venus, the Earth–Moon system, Mars, and the main asteroid belt. This process is difficult to study in its entirety because of the vast range of mass, time, and distance scales involved. Terrestrial planet formation is therefore broken up into several discrete stages.

Early on, the largest bodies in the swarm tend to grow fastest, in a process known as runaway growth, on a timescale of 10^4–10^6 y (Greenberg et al., 1978; Wetherill, 1980, 1990; Lissauer and Stewart, 1993; Wetherill and Stewart, 1989, 1993; Kokubo and Ida, 1996; Weidenschilling et al., 1997). When the largest bodies in the swarm grow large enough to dominate the dynamics of the disk through gravitational scattering, their growth slows down, and runaway growth transitions to oligarchic growth (Kokubo and Ida, 1998, 2000, 2002; Kominami and Ida, 2002; Thommes et al., 2003; Leinhardt and Richardson, 2005; Leinhardt et al., 2009; Levison et al., 2010).

The end result of this classic model of embryo growth is an "oligarchy" of many large embryos (10^{-2} to 10^{-1} $M_\oplus$, where $1\ M_\oplus = 6 \times 10^{27}$ g), separated in semimajor axis by $\sim 10 R_H$, where $R_H = a(M/3\ M_\odot)^{1/3}$ is Hill's radius, and containing half the mass of solids in the disk (Kokubo and Ida, 1998). The process of planet-formation then transitions to late-stage accretion, when over a period of several 10^7 years, growth of bodies is dominated by chaotic embryo–embryo mergers (Wetherill, 1985, 1990, 1992; Agnor et al., 1999; Chambers, 2001; Kominami and Ida, 2002; Nagasawa et al., 2005; O'Brien et al., 2006; Kenyon and Bromley, 2006; Raymond et al., 2005, 2006, 2009).

The study of terrestrial planet formation has advanced considerably in the past decade with improvements in computing power (e.g., O'Brien et al., 2006; Raymond et al., 2009). Simulations of the late-stage accretion generally result in terrestrial planet systems that broadly resemble our own. For instance, simulations can produce systems that match the observed orbital excitation of the terrestrial planets, as measured by their angular momentum deficit (AMD), in contrast with the previous generation of simulations (c.f. Brasser, 2013). Nevertheless, many important problems in terrestrial planet formation remain unsolved. In particular, the small sizes of both Mercury and Mars are difficult to produce in conventional models of terrestrial planet formation (Wetherill, 1991; Chambers, 2001; Raymond et al., 2009; Morishima et al., 2010).

Various researchers have addressed these specific discrepancies between terrestrial planet formation model outcomes and observations. However, the majority of simulations of the late-stage accretion take as their initial conditions the system of embryos and planetesimals that result from the "classic" runaway-to-oligarchic growth stage, which assumes that embryos grow by accreting mass from their local feeding zone. These earlier stages are modeled either using analytical or semi-analytical techniques (Weidenschilling, 1977a; Greenberg et al., 1978; Wetherill and Stewart, 1989), hybrid Monte Carlo and N-body codes (Spaute et al., 1991; Weidenschilling et al., 1997; Bromley and Kenyon, 2006; Kenyon and Bromley, 2006), or very limited fully N-body simulations (Kokubo and Ida, 1996, 1998, 2000). The results of a study in these early stages have typically lead to the initial conditions used in studies of late stage accretion. Here we show how the addition of PDM could potentially alter the distribution of mass at the start of late stage accretion.

There are two main limitations in the earlier simulations that have prevented PDM from occurring. The first limitation is one of resolution. In Section 2.2 we show that migration occurs when an embryo is $\gtrsim 100\times$ the mass of a typical local background planetesimal. When the mass ratio between embryos and disk planetesimals is less than $\sim$100, embryo motion is stochastic, and embryos random walk in semimajor axis. When the mass ratio is above this limit, embryo motion is relatively smooth and monotonic. In a terrestrial planet simulation, this requires a large number of simulated planetesimals in order to properly model the full disk, and typically simulations involving embryos embedded in planetesimal disks use planetesimals larger than 1/40 the mass of the embryos (O'Brien et al., 2006; Raymond et al., 2009).

The second limitation involves assumptions about how embryos are initially distributed in the protoplanetary disk. An embryo will only migrate if it is able to travel through an embryo-free zone of the disk, a criterion that we will quantify in Section 2.3.5. This requires that embryos form in some places in the disk before others—a situation that arises in simulations of runaway and oligarchic growth (Weidenschilling et al., 1997; Thommes et al., 2003). However, for reasons described above, N-body models of late-stage accretion take as their initial conditions a situation in which all embryos throughout the terrestrial planet region have already formed throughout the disk (Chambers and Wetherill, 1998; Agnor et al., 1999; Chambers, 2001; O'Brien et al., 2006; Raymond et al., 2009).

2. Quantifying the planetesimal-driven migration process

Planetesimal-driven migration can be understood in the following way. A close encounter between a single small planetesimal and much larger body (such as a planet or planetary embryo) can either increase or decrease the orbital angular momentum of the planetesimal and inversely that of the larger body. Whether the planetesimal experiences an increase or a decrease in orbital angular momentum depends on details of the encounter. Once a planetesimal begins to scatter off the large body, it will tend to continue scattering. Scattering will only halt if (1) the planetesimal impacts the large body, (2) it is ejected from the Solar System, (3) drag forces remove it from the region of influence of the large body, (4) it scatters off another nearby large body, or (5) the large body drifts a significant distance in semimajor axis between scatterings, thereby moving beyond the reach of the particle.

The large body tries to set up a steady state situation where it is scattering an equal mass of planetesimals inward as outward. Any imbalance in the mass of planetesimals that are scattering inwards compared to the mass of planetesimals that are scattering outwards will cause a net angular momentum transfer between the planetesimal disk and the large body. This results in a drift of the large body's semimajor axis, either inwards or outwards in response. Several factors can influence the direction of migration. Kirsh et al. (2009) showed that, in the absence of gas, an isolated embryo in a cold planetesimal disk starting from a stationary orbit will tend to migrate inward. However, such an idealized situation likely never occurs in nature. For instance, when two embryos are embedded in a planetesimal disk, they tend to repel each other (Kokubo and Ida, 1995). In addition, migration in either direction is self-sustaining, meaning that once a large body begins migrating in one direction it tends to keep moving in that direction (Kirsh et al., 2009). And so, the outermost embryo of a population will tend to migrate outward, away from its inward neighbors.

The self-sustaining nature of the direction of migration is due in part to the nature of the planetesimal disk on either side of the migrating body. When a large body scatters planetesimals in its neighborhood, the scattering process excites planetesimals and increases their eccentricity in a specific way. The Tisserand parameters of the planetesimals, defined relative to the large body's semimajor axis a_p as $T_p = a_p/a + 2\sqrt{a/ap(1-e^2)}\cos i$, is approximately conserved through scatting, so that after scattering planetesimals' new a, e, and i are constrained to a surface. On a plot of a versus e, these surfaces have the appearance of two "tails" that point out and away from the large body. If the large body is migrating (either inward or outward), then it moves away from the whichever tail is on its trailing side. Therefore the migrating body

will always have fewer planetesimals available for scattering on the side trailing its migration compared with its leading side, and this bias will lead to self-sustained migration.

Ida et al. (2000) showed that as long as the migration timescale was high relative to the scattering timescale within the migrating body's feeding zone then migration should be self-sustained. This implies that the mass of the migrating body must be smaller than its isolation mass in order to sustain migration. Kirsh et al. (2009) showed that there was a very strong bias that favored inward migration of isolated embryos, but also found that outward migration, once initiated, was self-sustaining albeit with a reduced migration rate. They hypothesize that the bias toward inward migration, and the consequent lower migration rate for outward migration, is due to the longer synodic period of planetesimals in the outer feeding zone relative to the inner one. That is, more encounters result in a transfer of planetesimals from the inner feeding zone to the outer on average, therefore drawing the migrating body toward the Sun. They also showed that the strength of this bias was a function of the migrating body's Hill radius, which were much larger for the giant planets in their study than for the terrestrial planet embryos in ours. In the PDM simulations of terrestrial planet embryos described below, we did not find a measurable direction bias in the migration rate.

2.1. The migration rate of inner Solar System embryos

An important quantity for understanding PDM is the migration rate. In order to place PDM in context with the planet formation process, it is useful to understand how the migration rate is affected by properties of the planetesimal disk. First, we will look at how the migration rate of an embryo is related to the surface mass density of the planetesimal disk. Ida et al. (2000) estimated the maximum migration rate assuming only the outer scattering zone is populated with scattering planetesimals. This is called the fiducial migration rate, given as:

$$\left|\frac{da_p}{dt}\right|_{fid} = \frac{a_p}{T_p}\frac{4\pi\Sigma_m a_p^2}{M_\odot}, \tag{1}$$

where T_p is the orbital period of the body at semimajor axis a_p in a planetesimal disk with surface mass density Σ_m. Note that the fiducial migration rate is independent of the mass of the planet. Kirsh et al. (2009) found that this fiducial migration rate is effectively an upper limit, and the observed rate of migration in N-body simulations is 0.2–0.7× the fiducial rate. This rate also assumes that the eccentricity of the planetesimal disk is relatively low.

An important quantity in setting the migration rate is the surface mass density of planetesimals, Σ_m. As we attempt to understand the role of PDM in the formation of rocky planets, we must adopt a model for the surface mass density of our planet-forming disk. In this paper mainly we use as our disk model some variant of the so-called "minimum mass solar nebula" (MMSN), a common starting point for almost all planet formation modeling (Weidenschilling, 1977b). This can be expressed as:

$$\Sigma_m(r) = \Sigma_{s,1\mathrm{AU}}(r/1\ \mathrm{AU})^p, \tag{2}$$

where r is the radial distance from the Sun, and $\Sigma_{s,1\mathrm{AU}}$ is the surface mass density of solids at 1 AU. The MMSN is derived by "reconstructing" the nebular disk that formed the planets using the present masses and distances from the Sun of the planets. A power law fit to the resulting surface mass density of matter from this reconstructed disk has values of $p = -1.5$, and a gas surface mass density and rock-forming solid surface mass density of $\Sigma_{g,1\mathrm{AU}} = 1700$–$3200\ \mathrm{g\ cm^{-2}}$ and $\Sigma_{s,1\mathrm{AU}} \approx 6$–$10\ \mathrm{g\ cm^{-2}}$, respectively (Weidenschilling, 1977b; Hayashi, 1981). However, caution is noted because the MMSN is empirically derived with the assumption that the present mass distribution of the planets reflects the mass distribution of the protoplanetary disk at some time.

While this type of disk profile is often used as a starting point for planet formation studies, the concept of the MMSN must be treated with some caution. Protoplanetary disks are dynamic environments, far too spatially and temporally complex to reduce to a single power law surface mass density description (c.f., Armitage, 2010). Nevertheless, the MMSN model is as good a starting point as any, and with only a few parameters to vary in this simple disk model (solid mass, gas mass, and a power law profile p) we can investigate the relevant dependences more clearly than with a more complex disk model.

We will adopt $\Sigma_{s,1\mathrm{AU}} = 8\ \mathrm{g\ cm^{-2}}$ as our canonical value for a $1\times$ MMSN disk. Because the gas-to-solid ratio at the mid-plane of the disk is poorly constrained, we will use a both $1700\ \mathrm{g\ cm^{-2}}$ and $3200\ \mathrm{g\ cm^{-2}}$ for $\Sigma_{g,1\ \mathrm{AU}}$ (Capobianco et al., 2011). Observations of disks around young stars as well as some numerical simulations of disk evolution suggests that protoplanetary disk surface mass density profiles might be better described with a slope of $p = -1.0$ (Andrews et al., 2010). Therefore, we will also consider how our results depend on these two different forms of the disk surface mass density slope.

Another important quantity that sets the migration rate of an embryo is the amount of mass available for it scatter. PDM is driven by the exchange of orbital angular momentum between the planetesimal disk and the embryo. This exchange can only be significant if the instantaneous total mass of planetesimals being scattered by the embryo is an appreciable fraction of the embryo's mass. The collective mass of planetesimals being scattered by the embryo is called the encounter mass, M_{enc}, given by:

$$M_{enc} \approx 5\left(\frac{M_p}{3M_\odot}\right)^{1/3}\pi\Sigma_m a_p^2. \tag{3}$$

Kirsh et al. (2009) found that there is a transition from a fast migration regime (where da_p/dt does not depend on M_p/M_{enc}) to a slow migration regime (where da_p/dt does depend on M_p/M_{enc}). They derived an empirical fit to the fiducial migration rate that captures this transition, given by:

$$\frac{da}{dt} \approx 0.5\left(\frac{da}{dt}\right)_{fid}\left[1+\frac{1}{5}\left(\frac{M_p}{M_{enc}}\right)^3\right]^{-1}. \tag{4}$$

How a migrating embryo transitions between the fast and slow regimes will be important for constraining the conditions under which PDM can operate on growing embryos in the inner Solar System.

2.2. N-body simulations of planetesimal-driven migration of isolated embryos

In this section we begin to develop our criteria for PDM. Recall that our plan is to run our new accretion code, *GAME*, described in Section 3 and Appendix A, and look for objects that should migrate based on these criteria. We begin to get insight into PDM by performing a series of simulations similar to those of Kirsh et al. (2009), but for embryos in the inner Solar System rather than ice giant/gas giant cores in the outer Solar System. This allows us to compare and contrast the behavior of migrating terrestrial planet embryos with that of giant planets, which most previous studies of PDM have focussed on.

We simulated PDM for isolated embryos with mass M_p ranging from $10^{-3}\ M_\oplus$ to $10^{-1}\ M_\oplus$, where $1\ M_\oplus = 6\times10^{27}$ g, in a disk of planetesimals using a parallelized implementation of the SyMBA integrator (Duncan et al., 1998). The full N-body dynamics of a swarm of planetesimals is challenging to compute because the number of computations goes as $\mathcal{O}(N^2)$. For numerical expediency,

SyMBA introduces a class of particles that only interact or collide with a small number of larger bodies, but not with each other, thereby reducing the number of computations needed to approximately $\mathcal{O}(N)$. Thus, with this class of small particle, the collective effects of a swarm of planetesimals on a massive body can be investigated in a computationally efficient way. This is a standard practice that is commonly used in simulations of embryos or planets that interact with massive planetesimal disks (e.g. Tsiganis et al., 2005; Morbidelli et al., 2005; Gomes et al., 2005; Kirsh et al., 2009; Raymond et al., 2009; Batygin and Brown, 2010; Nesvorný and Morbidelli, 2012).

The planetesimal disks were generated using the surface mass density formulation of Eq. (2), with $p = -1.5$, but with $\Sigma_{s,1\ \mathrm{AU}}$ varying between 8 and 24 g cm^{-2} (1–3 × MMSN). Each simulation initially contained $\sim 10^4$–10^5 planetesimals with bulk densities of 3 g cm^{-3}, which corresponds to diameters between ~200 and 600 km. The eccentricities (e) and inclinations (i) of the particles were taken from a Rayleigh distribution, where the RMS means were $\langle \bar{e} \rangle = 2\langle \bar{i} \rangle = 2 \times 10^{-3}$. For an embryo with a mass of 10^{-2} M$_\oplus$, this value of the eccentricity is what we define as the Hill scaled eccentricity, ε, where

$$\varepsilon = e_{RMS} R_H / a. \tag{5}$$

This puts the simulation in the regime where the migration rate is the fiducial rate given by Eq. (1), based on the simulations of Kirsh et al. (2009). The ratio of the RMS means of $\langle \bar{e} \rangle / \langle \bar{i} \rangle = 2$ is the based on equipartition of energy in a self-excited planetesimal disk (Ida and Makino, 1992). The remaining orbital angles were taken from a uniform distribution. The embryo was placed on an initially circular orbit at either 1.00 AU or 1.25 AU and each simulation was run for 10^5 y. The global integration stepsize for each simulation was 0.02 y.

We estimated the instantaneous migration rate as a function of time for each simulation. We do this because, as we will show, the relative growth rate of small inner Solar System embryos undergoing PDM is quite large, and therefore migrating embryos easily cross from the fast to the slow migration regimes in a single simulation. To determine the instantaneous migration rate of our embryo, we first performed a least squares fit of the a versus t history of the embryo in each simulation to an 8th order polynomial of the form $a_p(t) = \sum_{i=0}^{8} \alpha_i t^i$. We then take the first derivative of the fitted function to obtain an estimate of the migration rate as a function of time. The choice of an 8th order polynomial is arbitrary, but we found through experimentation that it is a high enough order to capture some of the stochastic nature of the N-body simulations, while low enough that it the fitted function and its first derivative is well behaved.

Using the M_p versus t history of each embryo, we can plot da_p versus M_p/M_{enc}. We have plotted Eq. (4) along with the polynomial fits to our simulation results in Fig. 1. Each curve in Fig. 1 is from a separate simulation, and the migration rate has been normalized to the fiducial rate given by Eq. (1). The dashed line is the empirical fiducial rate as a function of the ratio M_p/M_{enc} given by Eq. (4). Our agreement is good except at large mass ratios.

Our embryos grow relatively rapidly in our simulations and, as can be seen in Fig. 1, an embryo can grow more than an order of magnitude in mass, and. We find that the mass growth rate and the migration rate are correlated and can be expressed as:

$$\frac{dM_p}{dt} = \frac{\pi}{10} \left| \frac{da_p}{dt} \right|_{fid} \Sigma_m a_p. \tag{6}$$

We performed sensitivity tests with a range of bulk densities and found no major density dependence on the migration rate or growth rate. Embryos migrate at about 0.5× the fiducial rate, given by Eq. (1), until their $M_p/M_{enc} \approx 2$. Once a migrating embryo reaches $M_p/M_{enc} \approx 3$–4, PDM ceases to operate and the embryo remains nearly stationary. In some of our simulations, embryos migrated inward and in others they migrated outward. We plot the tracks of inward-going embryos as green lines in Fig. 1, and outward-going ones as black lines. Although Kirsh et al. (2009) found that outward migration for giant planets was approximately 34% slower than inward migration, we see no significant difference between the migration rate for inward going vs. outward going bodies in our simulations.

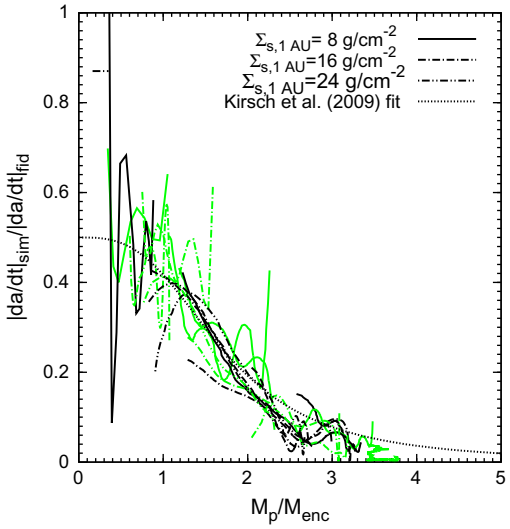

Fig. 1. Migration rate normalized to the fiducial rate given by Eq. (1) as a function of the embryo mass to encounter mass ratio M_p/M_{enc}. The migration rate for each simulation (which are represented as different cures in the figure) was found by fitting an 8th order polynomial to the a versus t history of the embryos, and then taking the derivative of the fitted function. The dashed lines are the empirical fiducial migration rate given by Eq. (4). Simulations where migration was inward are drawn with green lines, and those where migration was outward are drawn with black lines. We find no substantial difference between simulations with inward vs. outward migration. (For interpretation of the references to color in this figure legend, the reader is referred to the web version of this article.)

2.3. The five criteria for planetesimal-driven migration

In the previous section we demonstrated that isolated inner Solar System embryos can migrate via PDM, experience substantial growth during migration, and then halt when the ratio M_p/M_{enc} reaches ~3. While the simulations described above are useful to study some basic properties of PDM, they do not fully capture the complexity of embryo behavior in real systems. In particular, the initial conditions of the above simulations do not resemble the outcomes of earlier stages of planet formation. They assume that there is only one embryo in a system, and that it had grown to 10^{-2} M$_\oplus$ before it could suddenly begin to migrate.

Ideally in order to understand what role PDM will play during planet formation, we would want to study both the growth of bodies through accretion and the migration process with a single code. Unfortunately, this is not technically feasible because the number of particles needed to correctly model the growth of embryos out of a disk of planetesimals is so large that we cannot model the N-body gravitational dynamics with currently available computing hardware. Therefore we perform the calculations in steps, the first of which requires that we identify the necessary and sufficient criteria that must be met in order for PDM to occur. We then apply these criteria as a test within a growth code (described in Section 3).

Toward the first step, we have identified five criteria that must be simultaneously met in order for PDM to occur. For clarity, we have named the five criteria as follows:

1. The mass ratio criterion.
2. The mass resolution criterion.
3. The disk eccentricity criterion.
4. The crowded criterion.
5. The growth timescale criterion.

In the following subsections, we will describe each of these criteria in detail.

2.3.1. The mass ratio criterion

Migration will stall if the ratio $M_p/M_{enc} \gtrsim 3$, where M_p is the mass of the embryo and M_{enc} is the total mass of planetesimals being scattered (Kirsh et al., 2009). We have confirmed this result in our own simulations in Section 2.2, as shown in Fig. 1. Using the estimate of M_{enc} given by Eq. (3), the mass ratio criterion can be expressed in terms of a stopping mass, M_{stop}, as:

$$M_{stop} \approx \left[15\pi(3M_\odot)^{-1/3}\Sigma_s a_p^2\right]^{3/2}. \quad (7)$$

If the embryo grows larger than M_{stop}, it will be unable to experience PDM. The PDM stopping mass is equivalent to the isolation mass, which is the largest mass that an embryo can achieve in oligarchic growth before it depletes its feeding zone of planetesimal mass (Lissauer, 1987; Bryden et al., 2000). The isolation mass is given by:

$$M_{iso} = 4\pi\Sigma_s a_p^2 \Delta_M, \quad (8)$$

where Δ_M is the characteristic spacing of embryos. If we take $\Delta_M = bR_H$, where R_H is the radius of the embryo's Hill's sphere, and b is a multiplicative factor, then we can rewrite Eq. (8) as:

$$M_{iso} = \left[4b\pi(3M_\odot)^{-1/3}\Sigma_s a_p^2\right]^{3/2}, \quad (9)$$

which is identical to Eq. (7) for $b = 15/4$.

In Fig. 2 we plot Eq. (7) as a function of semimajor axis for four different disk models. All disk models conform to Eq. (2), although we have included the effects of a "snowline," beyond which Σ_s is enhanced by a factor of 4 due to the condensation of ices. We have placed the snowline at 2 AU in our disks. The solid lines in Fig. 2 correspond to a 1 × MMSN disk ($\Sigma_{s,1AU} = 8$ g cm^2), with $p = -1.5$ (black curves) and $p = -1.0$ (red curves). The growth of giant planet cores within the lifetime of the gas disk may require as much as 10× the surface mass density as the MMSN value (Thommes et al., 2003), and therefore we have also included a 10 × MMSN disk ($\Sigma_{s,1AU} = 80$ g cm^2) as the dashed lines in Fig. 2. For the inner Solar System, we find that M_{stop} is typically $\lesssim 10^{-1}$ M$_\oplus$ for a standard minimum mass solar nebula (MMSN) disk model with $\Sigma_{m,1AU} = 8$ g cm^{-2}.

In the outer Solar System, M_{stop} can be larger, and objects can migrate even when they are of the order of 10 M$_\oplus$, which is the similar to the estimated masses of the cores of giant planets (Mizuno et al., 1978; Pollack et al., 1996; Hubickyj et al., 2005). This is perhaps not surprising considering that the PDM stopping mass is equivalent to the isolation mass, as shown in Eqs. (7) and (9). Because the core accretion model for giant planets requires cores to reach a mass of ~10 M$_\oplus$ in order to initiate runaway gas accretion, any disk capable of producing giant planet cores through oligarchic growth (e.g. Thommes et al., 2003) will also potentially allow those cores to migrate via PDM. It may even be difficult to build giant planet cores at all without PDM (Levison et al., 2010).

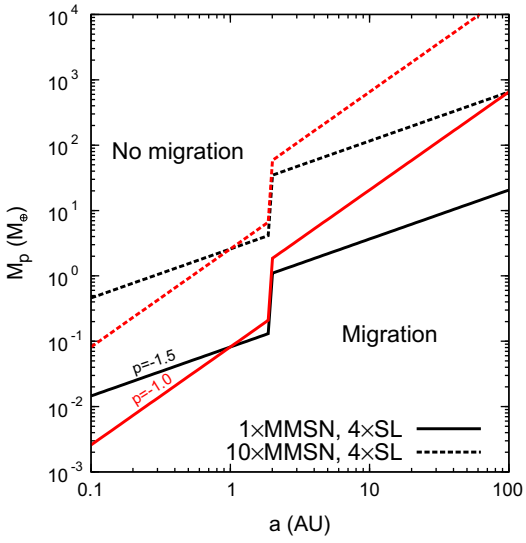

Fig. 2. Migration halting mass, defined as $M_p/M_{enc} = 3$, as a function of semimajor axis and disk surface mass density and slope of the surface mass density function. Migration will not occur for M_p values greater than those shown by the dotted lines. The disk surface mass density is a power law defined by Eq. (2) with $p = -1.5$ (black lines) and $p = -1.0$ (red lines). We have also included the effects of a "snowline," beyond which Σ_s is enhanced by a factor of 4 due to the condensation of ices. We have placed the snowline at 2 AU in our disks. The solid lines correspond to a 1 × MMSN disk ($\Sigma_{s,1\ AU} = 8$ g cm^2). The growth of giant planet cores within the lifetime of the gas disk may require as much as 10× the surface mass density as the MMSN value (Thommes et al., 2003), and therefore we have also included a 10 × MMSN disk ($\Sigma_{s,1\ AU} = 80$ g cm^2) as the dashed lines. (For interpretation of the references to color in this figure legend, the reader is referred to the web version of this article.)

2.3.2. The mass resolution criterion

As we noted in Section 1.1, typical late-stage numerical simulations take the initial mass ratio between planetesimal and embryos to be 1/40 (O'Brien et al., 2006; Raymond et al., 2009). Here we explored the dependence of the ability of the embryo to migrate on the mass ratio between an embryo and the background planetesimals. Six simulations were performed with similar initial conditions, varying only the masses of the individual planetesimals. In these simulations, an embryo with a mass of 10^{-2} M$_\oplus$ was placed at 1.25 AU, surrounded by a disk of planetesimals with a surface mass density given by Eq. (2) and $\Sigma_{s,1AU} = 16$ g cm^{-2} (2 × MMSN). The number of particles in the simulation was varied so that the initial ratio of M_p/m varied between 41 and 354, where M_p is the mass of the embryo and m is the mass of an individual planetesimal.

Fig. 3 shows that when $M_p/m \gtrsim 100$, the embryo's motion in the disk is monotonic throughout the simulation, and so PDM occurs. Below this value of the mass ratio, the motion of the embryo is much more chaotic. Thus, we adopt $M_p/m > 100$ as our second criterion.

2.3.3. The disk eccentricity criterion

Kirsh et al. (2009) found that the migration rate was roughly constant as a function of the eccentricity divided by the Hill factor, defined as $\varepsilon = e_{RMS}a/R_H$, for $\varepsilon \lesssim 3$. We use a cutoff value of $\varepsilon = 5$ for our criterion, as this is when the migration rate has dropped by roughly a factor of 10 (Kirsh et al., 2009).

2.3.4. The crowded criterion

Bromley and Kenyon (2011) claimed that PDM should not occur during planet formation because embryos growing within the planetesimal disk will be crowded together with other similar-sized embryos. Whether this is true or not should depend, in detail,

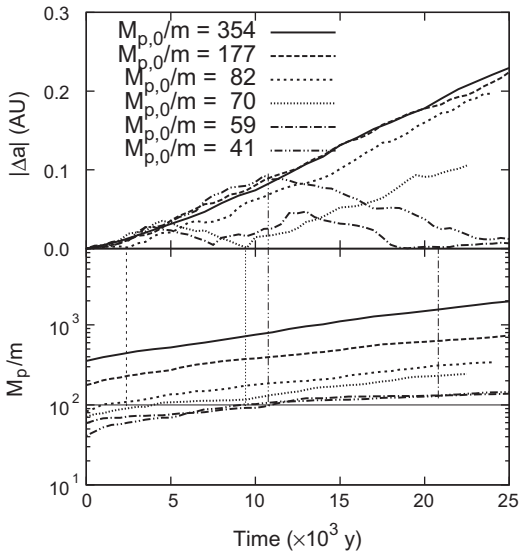

Fig. 3. Effect of simulation resolution on migration behavior. Six simulation results are shown for a 0.01 $M_\oplus$ embryo embedded in a 2 × MMSN disk of planetesimals of varying masses. The disk spanned from 1.0 to 1.5 AU, and the embryo was initially placed at 1.25 AU. The different lines correspond to different values of the initial embryo mass ($M_{p,0}$) to planetesimal mass (m) ratio. The upper panel shows the absolute value of the migration distance relative to its starting location, and the lower panel shows instantaneous embryo to planetesimal mass ratio. A body that changes direction is not exhibiting monotonic migration. By matching up a line in the upper panel at the moment of a direction change with its corresponding line in the lower panel, the value of M_p/m which fails to exhibit monotonic migration is determined. To guide the eye, we have drawn lines connecting the point where the last direction change occurred in the upper panel, to the corresponding value of the mass ratio in the lower panel. Monotonic migration was only observed when the mass ratio $M_p/m \gtrsim 100$. In the simulation where the initial $M_p/m = 59$, it is difficult to determine if monotonic PDM ever got established. However, this body never reached a $M_p/m > 150$.

on the mass ratio between an embryo and its nearest neighbors. If the neighbors are of similar mass, then scattering between the embryos should prevent migration. However, if the embryo that could potentially migrate is large relative to its neighbors, then scattering by the neighbors will be ineffective in preventing migration, so that PDM will occur. We have quantified where this transition takes place using SyMBA.

In particular, the purpose of the following numerical experiment is to determine the critical mass ratio between an embryo and its nearest-neighbor embryo that allows the larger embryo to migrate past the smaller one instead of being scattered. This is different than the mass resolution criterion described in Section 2.3.2. For that criterion, the critical mass ratio was the ratio between the embryo and the numerous small planetesimals that drive PDM. Here we are concerned with a small number of embryo–embryo interactions.

In a SyMBA run, a 10^{-2} $M_\oplus$ embryo, designated M_p, is embedded at 1 AU in a disk of planetesimals. The embryo and planetesimals have a mass ratio $Mp/m = 300$ in order to satisfy the mass resolution criterion. To satisfy the mass ratio criterion, the disk surface density profile, which is spread from 0.9 to 1.8 AU, is set by Eq. (2), with $\Sigma_{s,1AU} = 16$ g cm^{-2} and $p = -1.5$. The embryo has a smaller neighbor that is placed at 1.16 AU, and whose mass varies between simulations from 0.05 to 0.2×10^{-2} $M_\oplus$. The small embryo is far enough away from the large one that the latter can establish PDM before it encounters its neighbor. In addition, an outward force is applied to the largest embryo for the first 10^{-2} AU of the simulation to cause it to migrate at a rate equal to the fiducial rate given by Eq. (1). This is done so that the large embryo is migrating toward its smaller neighbor. The global integration stepsize was 0.02 y.

When the two embryos encounter each other, the larger embryo may either continue migrating or reverse direction. We plot in Fig. 4 the ratio M_p/M as a function of semimajor axis at the moment when the two embryos encounter each other, where M is the mass of the smaller embryo and M_p is the mass of the larger one. If the larger embryo migrates past the smaller one we plot it as a solid square. If instead the larger embryo is repelled by the smaller one, then we plot it as an open circle. A smaller embryo is not expected to migrate past a larger one. We see that the larger embryo is able to migrate past bodies with $M_p/M \gtrsim 10$, but can be hindered by bodies with $M_p/M \lesssim 5$—10. Therefore, we take as our criterion that an embryo may only migrate if it is at least 5–10× more massive than any other objects it encounters within its scatting zone. We take as the width of the scattering zone an annulus of $3R_H$ in the direction of migration (Kirsh et al., 2009).

2.3.5. The growth timescale criterion

In order to be complete, we must also consider the growth of new embryos along the outward-going trajectory of the migrating bodies. An embryo must be able to migrate through the disk unencumbered by newly-formed like-sized embryos. Up to now, we have considered migration criteria that apply to individual objects in a static disk with the aim to discern whether or not they are capable of migration. The growth timescale criterion, however, depends on how objects in the *rest* of the disk are growing, and therefore a somewhat different approach is warranted.

Our migration criterion can be quantified by comparing the timescale for migration, τ_{mig}, with an appropriate timescale that can characterize embryo growth, τ_{grow}. The timescale for migration is $\tau_{mig} = a/|\dot{a}_{mig}|$, where we use the approximation $\dot{a}_{mig} \approx 0.5 da/dt_{fid}$, and da/dt_{fid} is given by Eq. (1). The factor of 0.5 is applied based on the results of our simulations shown in Fig. 1.

To develop an embryo growth timescale, τ_{grow}, that can be directly compared to τ_{mig} is somewhat more complicated. It is useful to think about the formation of embryos as an outwardly propagating "front." At any given time a semimajor axis exists where the

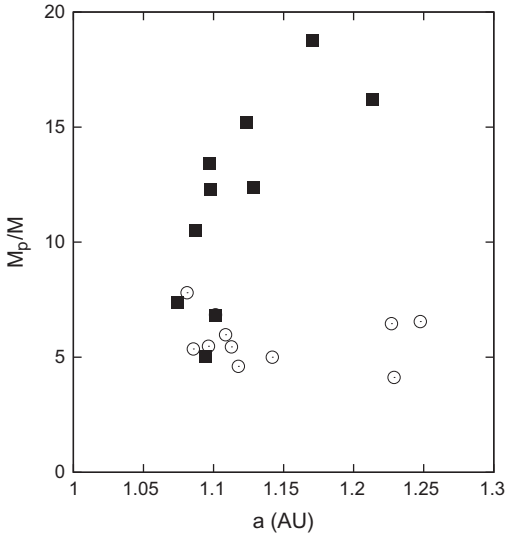

Fig. 4. Results of SyMBA simulations showing results of encounters between pairs of embryos. In these simulations the larger embryo, with mass M_p, migrates via PDM toward the smaller one, with mass M. When the two embryos encounter each other, the larger embryo may either continue migrating or halt (or sometimes reverse direction). Plotted here are the ratios M_p/M versus semimajor axis at time of encounter for several pairs of embryos. Solid squares are cases where the larger embryo migrated past the smaller embryo. Open circles are cases where the larger embryo was repelled by the smaller embryo. Migration was hindered when the value of M_p/M was less than ~5.

largest object in the local swarm is some value that will hinder the migration of an embryo, which we call M_{large}. The value of M_{large} is difficult to calculate in general because it depends on the specific properties of a particular potentially migrating embryo. Nevertheless, we will assume that the typical value for M_{large} is the runaway-to-oligarch transition mass. We justify this assumption with the following argument. In the runaway growth mode, because $\dot{M}_p \propto M_p^{\gamma}$ and $\gamma = 4/3$, the masses of any two bodies who are initially nearly the same size will diverge (that is, larger objects grow faster than smaller ones) (Kokubo and Ida, 1996). In the oligarchic growth mode $\gamma = 2/3$, and so the masses of any two oligarchs will converge over time. Therefore, during runaway growth, the largest object will continue to build a size advantage over its neighbors. However, once the system transitions to oligarchic growth, any object that might have been able to migrate will begin to lose this advantage. Thus, the largest advantage will occur at the transition, which is precisely what we mean by M_{large}.

Ida and Makino (1993) estimated the mass ratio between a growing embryo and the mass of a typical planetesimal in the background swarm population at which the transition between these growth modes occurs:

$$\frac{M_{\rm large}}{m} \gtrsim 50 \times \left(\frac{m}{10^{23}\ {\rm g}}\right)^{-2/5} \times \left(\frac{a}{1\ {\rm AU}}\right)^{3/10} \times \left(\frac{\Sigma_m}{\Sigma_{s,std}}\right)^{-3/5}, \tag{10}$$

where we take $M_{\rm large}$ to be the mass of the embryo body at the transition, and m is the mass of a typical planetesimal. The above equation has also been normalized with a "standard" MMSN model where $\Sigma_{s,1\rm AU} = 10\ {\rm g\ cm^2}$ and $p = -1.5$. Because embryo growth is fastest in the innermost part of the planetesimal disk, the first embryos of mass M_{large} will form at the inner edge of the disk.

As time progresses, the semimajor axis where objects have reached the size M_{large} will move outward. The rate of outward propagation of this location is $(dT_{large}/da)^{-1}$, where T_{large} is the amount of time needed for runaway growth to produce an object of mass M_{large}.

Understanding the timescale for embryo growth requires a quantitative understanding the evolution of the protoplanetary disk through time. Therefore, first we must describe an analytical model for the growth of bodies within a planetesimal disk of the type first pioneered by Safronov (1972). For a number of years prior to the availability of inexpensive and powerful computer workstations capable of performing N-body simulations of planetesimal swarms, planet formation via accretion in planetesimal disks was studied using analytical and semi-analytical techniques. These techniques, despite their limitations, illuminated many important processes, and indeed the very concept of "runaway growth" was developed in this era (Greenberg et al., 1978; Weidenschilling, 1980). Even when N-body codes became widely available, analysis based on Safronov's coagulation theory were still employed, as for instance in understanding how runaway growth slows and transitions to oligarchic growth (Ida and Makino, 1993; Kokubo and Ida, 1998). In a coagulation model, the planetesimals are assumed to be in a regime where gravitational focussing and dynamical friction are both effective. Following Thommes et al. (2003), the growth rate of a body with mass M_p can be written as:

$$\frac{dM_p}{dt} \simeq C \frac{\Sigma_m M_p^{4/3}}{e_m^2 a^{1/2}}, \tag{11}$$

where $C = 6\pi^{2/3}\left[3/\left(4\rho_{M_p}\right)\right]^{1/3}[G/M_\odot]^{1/2}$, and ρ_M is the bulk density of the growing body. The planetesimal disk surface mass density is $\Sigma_m(a)$ and its RMS mean eccentricity is e_m. We can solve Eq. (11) for the time needed to reach M_{large} at semimajor axis a:

$$T_{large} = \frac{3e_m^2 a_p^{1/2}}{C\Sigma_m}\left(M_0^{-1/3} - M_{large}^{-1/3}\right), \tag{12}$$

where M_0 is the initial mass of the object that eventually becomes the embryo. We take the derivative of Eq. (12) with respect to a, and the embryo growth timescale is then $\tau_{grow} = a/(da/dT_{large})$.

For this calculation, we assume that the eccentricity of the planetesimal disk, e_m, is set by a competition between self-stirring by the planetesimals and stirring due to embryos, and damping by gas drag. It is therefore a complex function of semimajor axis and time, and depends greatly on models of the gas disk and collisional evolution of the planetesimals. During the runaway stage the planetesimal disk self-heats due to viscous stirring, that is planetesimal–planetesimal scattering will cause the e_{RMS} of the disk to increase over time. Planetesimal-embryo stirring is unimportant during the runaway stage because there are so few embryos. When the eccentricity and inclination growth in the disk is dominated by stirring of the few largest growing bodies, rather than self-stirring from the swarm of smaller bodies, then the system is, by definition, undergoing oligarchic growth.

From Ida and Makino (1993), the timescales for eccentricity growth due to self-stirring and stirring by oligarchs can be expressed as:

$$T_{VS}^{m-m} = \frac{1}{40}\left(\frac{\Omega^2 a^3}{Gm}\right)^2 \frac{m e_m^4}{\Sigma_m a^2 \Omega}; \tag{13}$$

$$T_{VS}^{M_p-m} = \frac{1}{40}\left(\frac{\Omega^2 a^3}{GM_p}\right)^2 \frac{M_p e_m^4}{\Sigma_{M_p} a^2 \Omega}, \tag{14}$$

where Ω is the Keplerian orbital angular velocity, and Σ_{M_p} and Σ_m are the surface mass densities of oligarchs and planetesimals, respectively. The transition between runaway and oligarchic growth occurs for M_p such that these two timescales are equal. Although we do not need Eq. (14) now, we will make use of it later in Section 3, and we include it here for completeness.

As described above, we assume the eccentricity growth due to stirring will be counteracted by damping due to gas drag. Following Thommes et al. (2003), the gas drag damping timescale is given by:

$$T_{gas}^{e_m} \simeq \frac{1}{e_m}\frac{m}{(C_D/2)\pi r_m^2 \rho_{gas} a\Omega}, \tag{15}$$

where $C_D \approx 1$ is the dimensionless drag coefficient, and ρ_{gas} is the gas volume density (Adachi et al., 1976). Assuming that the gas disk can be approximated as being in hydrostatic equilibrium with a temperature profile given as $T \propto r^k$ and a surface mass density profile $\Sigma \propto r^p$, then the gas density at the mid-plane is given as $\rho \propto r^{(p+k-3)/2}$ (Armitage, 2007). For typical values of $k = -1$ and $p = -3/2$ and the MMSN model values for gas $\Sigma_{g,1\rm AU} = 1700$–$3200\ {\rm g\ cm^2}$, then the MMSN gas volume density profile is $\rho(r) = \rho_0 r^{-11/4}$, where $\rho_0 = 1.4$–$2.7 \times 10^{-9}\ {\rm g\ cm^{-3}}$.

If we assume that the planetesimal disk is in an equilibrium state where viscous stirring and gas drag are in balance, then:

$$e_m|_{runaway} = \left[\frac{80}{\pi}\left(\frac{Gm}{\Omega^2 a^3}\right)^2 \frac{a\Sigma_m}{C_D r_m^2 \rho_{gas}}\right]^{1/5}; \tag{16}$$

In order to evaluate τ_{grow}, we plug Eq. (16) into Eq. (12). Note that we only need to consider the runaway growth regime because we defined M_{large} to be at the runaway-oligarchic growth boundary. The equivalent formulation for eccentricity in the oligarchic regime is

$$e_m|_{oligarchic} = \left[\frac{40}{\pi^2}\left(\frac{GM_p}{\Omega^2 a^3}\right)^2 \frac{m}{bR_H C_D r_m^2 \rho_{gas}}\right]^{1/5}. \tag{17}$$

Our last migration criterion therefore states that PDM can only occur if $\tau_{grow} > \tau_{mig}$. This means that the when this criterion is

satisfied, the embryo will be migrating outward faster than the accretion front, thus outrunning it.

It is important to note that, unlike the previous criteria, this is only a function of the characteristics of the disk itself and does not require that we perform a detailed Monte Carlo calculation of accretion before it is evaluated. The other criteria are local and thus they can be satisfied by an embryo that is lucky and becomes unexpectedly large due to a series of larger than "expected" mergers, which are further enhanced by during the runaway growth phase. However, it does not matter how lucky an embryo is for the growth timescale criterion; if the accretion front is expanding outward faster than the embryo can migrate, then the embryo will eventually run into a like-size object and PDM will stall. Note that we have not taken into account the additional growth that the embryo will experience due to the migration itself, as given by Eq. (6), and therefore this analysis may be conservative.

We can now compare τ_{mig} and τ_{grow}. Such a comparison is shown in Fig. 5 for a 1×, 2×, and 3 × MMSN planetesimal disk. These results were obtained for a disk model with planetesimals having a range of initial masses between 3×10^{-8}–2×10^{-6} $M_\oplus$ (corresponding to initial diameters between 50 and 200 km), similarly to what was used in Section 2.3.3. As the largest objects in the distribution grow fastest in the runaway growth mode, M_0 is taken to be the upper end of the mass range and m is taken to be the lower end of the range. The disk eccentricity used in Eq. (11) is obtained using Eq. (16) for the equilibrium eccentricity during runaway growth, and therefore these results depend on the profile of the gas disk.

As Fig. 5 shows, there is a semimajor axis beyond which τ_{grow} is longer than τ_{mig}, which we will say is the point where the embryos can migrate due to PDM faster than the outwardly-propagating front on new embryos. This means that embryos that form inward of this location will not be able to migrate fast enough to outpace the formation front of new embryos. Outward of this point, embryos migrate faster than the embryo formation front, and therefore PDM is possible. We plot the location beyond which PDM may be possible as a function of disk mass and for our two surface mass density profile slopes in Fig. 6. For the disk models we consider here, PDM becomes possible outward of ∼0.7—1.0 AU.

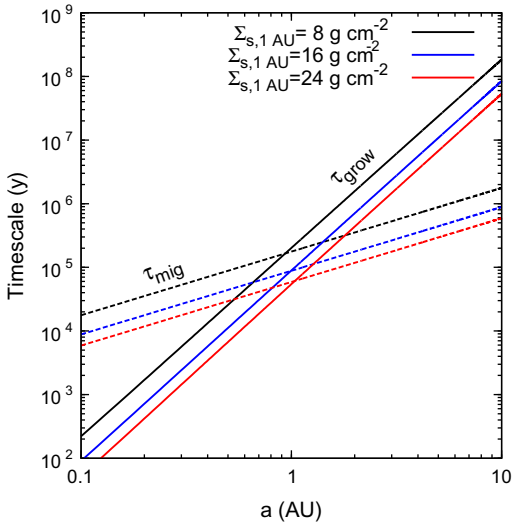

Fig. 5. A comparison of the embryo migration timescale with the embryo formation timescale as a function of disk mass, for disks with a profile given by Eq. (2) with $p = -1.5$. At locations in the disk where the embryo formation timescale is shorter than the embryo migration timescale migration will not be possible, because new embryos are able to form in-place before older embryos can migrate there. At locations where the migration timescale is shorter than the formation timescale, migrating embryos can reach regions in the disk that have not had time to produce new embryos in-place. With these disk conditions, embryos that form at $a \lesssim 0.7$ AU will not be able to migrate.

3. The onset of PDM in the terrestrial planet zone

We have now established five criteria that must be simultaneously met in order for PDM to occur. Next, for a given disk we must model the evolution of embryos to determine if any of them can migrate. Based on the growth timescale criterion described in Section 2.3.5, we do not expect embryos that form inward of ∼0.7–1.0 AU to migrate. Outward of this location, the crowded criterion described in Section 2.3.4 is perhaps the most substantial barrier to PDM. In order for PDM to occur, embryos must emerge that are 5–10× larger than their neighbors. Bromley and Kenyon (2011) propose that this cannot happen because growing oligarchs are always surrounded by like-sized bodies.

However, embryo growth via mergers is not a continuum process, it is discrete and stochastic. That is, bodies do not grow by some infinitesimal mass dM in some infinitesimal time dt, but rather mass changes in discrete jumps of ΔM whenever a merger happens to occur. Even if the initial planetesimal mass function (the initial size-frequency distribution of the planetesimals) is a delta function with a single intrinsic mass, random variations in merger frequency that must naturally occur will cause some planetesimals to grow slightly faster than others. During the runaway phase, when $dM/dt \propto M^{4/3}$, the differential growth rate will cause these mass differences to become magnified over time. On average dM/dt may be described approximately by Eq. (11), but because PDM occurs for the (locally) very largest bodies within the planetesimal disk, one must account for the stochastic variability in growth rate. To put it another way, it is not the "typical" embryo that potentially experiences PDM, it is a statistical outlier.

The difficulty of using N-body codes to study this process is that planetesimals are quite numerous. A $D = 100$ km planetesimal with a density of 2.5 g cm^{-3} has a mass of only 2×10^{-7} $M_\oplus$. This means that in order to simulate enough mass to make the terrestrial planets, one needs to simulate a minimum of $\sim 10^7$ planetesimals of this size. This is far beyond the capability of N-body codes at the present time. It is this problem that our

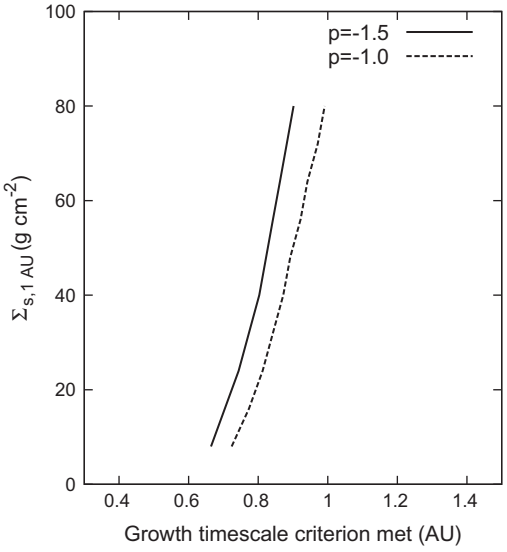

Fig. 6. Location beyond which the growth timescale criterion is met as a function of disk mass. $\Sigma_{s,1AU}$ is the surface mass density at 1 AU of the solid component of the disk (as opposed to the gas component).

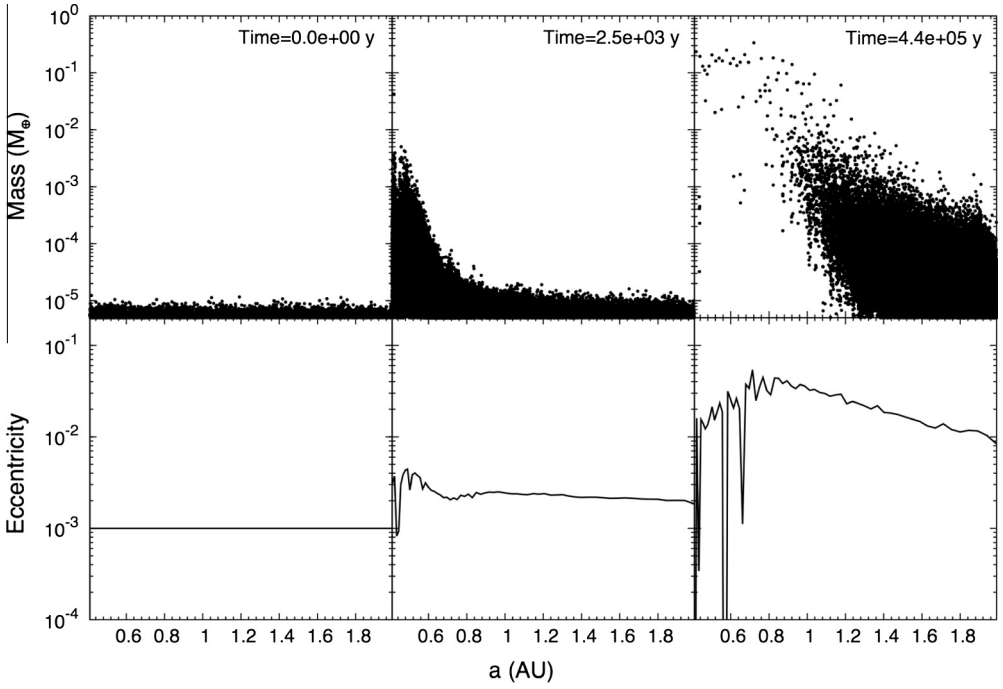

Fig. 7. Example output of a typical *GAME* run. This run is for a 4 × MMSN disk ($\Sigma_{s,1\ \mathrm{AU}} = 32\ \mathrm{g\ cm^{-2}}$, $p = -1.5$) for planetesimals with an initial mean mass $\overline{D}_i = 100$ km and dispersion of 50 km. The upper panels show the mass of planetesimals as a function of semimajor axis for three output times. The lower panels show the eccentricity of the disk at the same three output times.

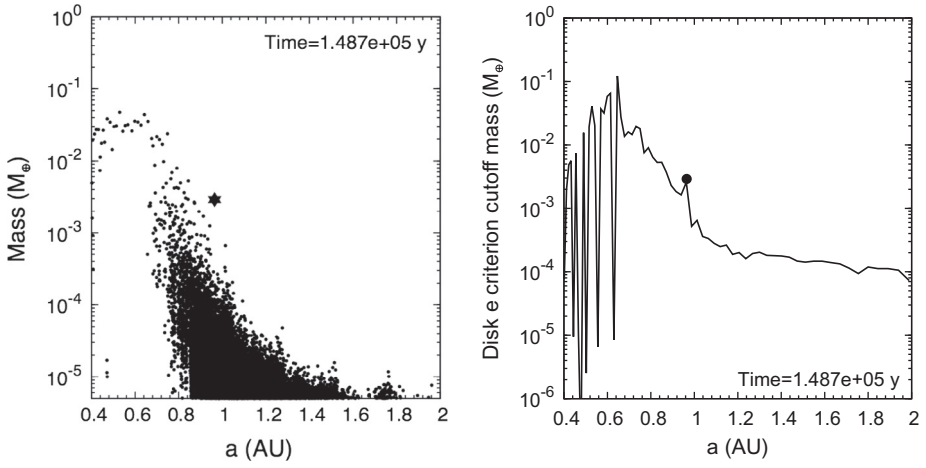

Fig. 8. Results from a *GAME* run at the time of the emergence of a migration candidate. Left panel: The mass of individual objects in the disk as a function of semimajor axis. The migration candidate is highlighted as a large star. Right panel: The mass cutoff for the disk eccentricity criterion as a function of semimajor axis for a disk in *GAME*. The mass cutoff is defined as $M_{cutoff} = 3\ \mathrm{M}_{\odot}\left(e_{RMS}/\varepsilon_{cutoff}\right)^3$. The circle plotted is the migration candidate, which just satisfies the disk eccentricity criterion at the time of emergence. This example comes from a run with $\Sigma_{s,1\ \mathrm{AU}} = 8\ \mathrm{g\ cm^{-2}}$, $\Sigma_g/\Sigma_s = 525$, $\overline{D}_i = 50$ km, and $p = -1.5$.

new Monte Carlo code *GAME* was designed to address. *GAME* stands for *Growth And Migration of Embryos*. The purpose of *GAME* is to simulate the evolution of a planetesimal disk in the presence of gas drag, at the level of individual planetesimals. Rather than simulate the N-body gravitational dynamics of this vast swarm of particles, which is too computationally expensive to be practical, *GAME* uses a Monte Carlo approach to simulate both the growth of planetesimals through mergers, while following velocity evolution of the disk using the analytical formalism captured in Eqs. (13)–(15). Planetesimals are simulated as individual bodies that grow by merging with their neighbors. Thus, they grow in discrete jumps, which, on average, approximate Eq. (11). Details of how *GAME* is implemented may be found in Appendix A.

Using *GAME*, we are able to identify "migration candidates," which are objects that satisfy each of the five migration criteria simultaneously. We performed a large number of simulations to determine how important disk parameters control the emergence of migration candidates, and their properties (such as mass and orbital semimajor axis) when they emerge. The disk parameters that we allowed to vary were the total solid disk mass ($\Sigma_{s,1\mathrm{AU}} = 8$–$32\ \mathrm{g\ cm^{-2}}$), the gas-to-solid fraction ($\Sigma_g/\Sigma_s = 212.5$–$525$, corresponding to our chosen range of mid-plane disk metallicity), and the initial mass function of the

Table 1
Results from a *GAME* parameter study.

$\Sigma_{s,1\ AU}$ (g cm^{-2})	Σ_g/Σ_s	$\overline{D}_i$ (km)	Number of runs N_c		N_{all}
8	212.5	100	10	0	0
8	212.5	50	10	5	5
8	525.0	100	10	1	1
8	525.0	50	10	4	2
16	212.5	100	10	1	1
16	212.5	50	10	15	10
16	525.0	100	10	3	3
16	525.0	50	10	14	10
24	212.5	100	10	5	2
24	212.5	50	10	19	14
24	525.0	100	10	7	4
24	525.0	50	10	26	18
32	212.5	100	10	11	5
32	212.5	50	10	20	15
32	525.0	100	10	10	8
32	525.0	50	10	39	31

N_c: Number of objects that satisfy the crowded criterion.
N_{all}: Number of objects that satisfy all four criteria.

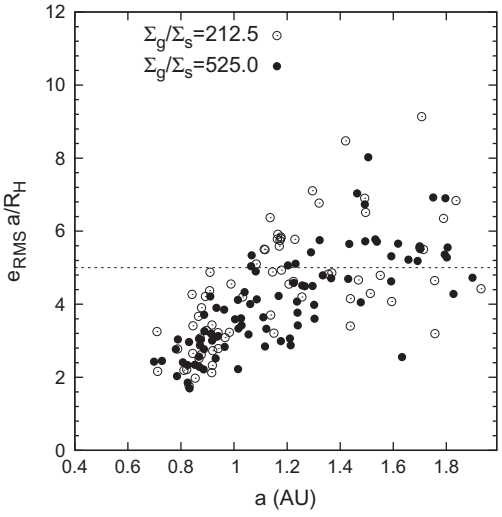

Fig. 9. *GAME* runs showing how meeting the disk eccentricity criterion is a function of the semimajor axis where the migration candidate emerges. Each point represents an object that has satisfied the crowded, mass ratio, and mass resolution criteria. The dashed line represents the disk eccentricity criterion cutoff. Objects above the line fail the disk eccentricity criterion and will not migrate. Closed circles represent simulations with our gas-to-solid ratio of 525, while the open circles represent simulations with our gas-to-solid ratio of 212.5.

planetesimals. Our chosen range mid-plane metallicity corresponds to the estimate range of gas density needed to produce the MMSN of $\Sigma_{g,1AU} = 1700$—4200 g cm^{-2} (Raymond et al., 2005)[1] divided by our "canonical" MMSN solid density $\Sigma_{s,1AU} = 8$ g cm^{-2}.

The initial mass function (initial size distribution) of the planetesimals is poorly constrained. The size distributions of large bodies in the Main Asteroid Belt as well as the cold classical Kuiper Belt suggest that they were initially highly depleted in objects with $D < 50$—100 km and that the size distribution above 100 km was very steep (Morbidelli et al., 2009; Fraser et al., 2008). This preference for large sizes is consistent with planetesimal formation by some type of gravitational instability or turbulent concentration

[1] The upper range of $\Sigma_{g,1AU} = 4200$ g cm^{-2} reported by Raymond et al. (2005) is taken from Weidenschilling (1977b). However, Weidenschilling (1977b) actually report $\Sigma_{g,1AU} = 3200$ g cm^{-2}, and therefore this appears to be a typo within the Raymond et al. (2005) paper.

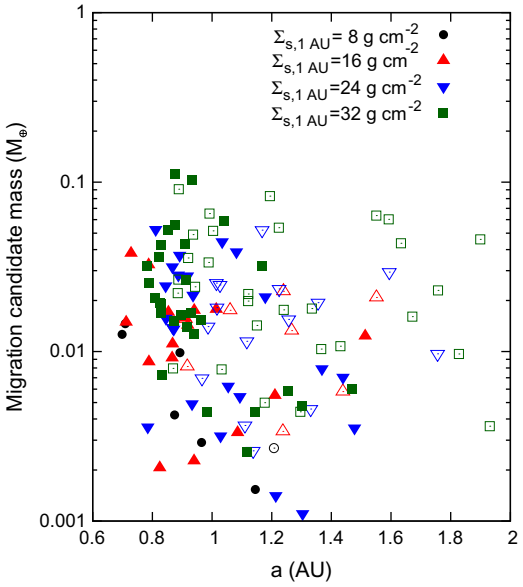

Fig. 10. *GAME* runs showing the mass and semimajor axis of objects that satisfy all five migration criteria simultaneously. Different colors are for *GAME* runs with different disk masses, where $1\times$ MMSN is equivalent to a disk with $\Sigma_{s,1AU} = 8$ g cm^{-2}. For runs that generate multiple candidates in the same run, the first occurrence of a migration candidate is indicated with a filled symbol, later occurrences are indicated with open symbols.

mechanism (see Chiang and Youdin, 2010, for a review), and with the formation of wide Kuiper Belt binaries (Nesvorný et al., 2010).

For simplicity, we have modeled our initial population of planetesimals as being derived from a normal distribution with a mean diameter, $\overline{D}_i$. For most of our runs we set the initial dispersion, σ_i, to be equal to $\frac{1}{2}\overline{D}_i$. We also explored three different values for dispersion, $\sigma_i = \frac{1}{4}$, $\frac{1}{2}$, and $\frac{3}{4}\overline{D}_i$, for the case where $\Sigma_{s,1AU} = 8$ g cm^{-2} and $\overline{D}_i = 50$ km. Based on resolution constraints in *GAME*, it is impractical to model disks with $\overline{D}_i \lesssim 50$ km. Therefore we only modeled two values of $\overline{D}_i$, 50 km and 100 km, which, according to Morbidelli et al. (2009), is consistent with the peak of the initial mass distribution in the asteroid belt. While Weidenschilling (2011) argues that the initial planetesimals may have been much smaller than this, as we will demonstrate with our *GAME* results, smaller initial planetesimals may make migrating embryos more likely. Thus the larger initial planetesimals used here may be somewhat conservative.

All disks in our *GAME* runs spanned the region from 0.4 to 2 AU and the planetesimals were modeled as rocky objects with density $\rho = 3$ g cm^{-3}. We ran 10 instances of *GAME* for each unique set of parameters, varying only the random number generator seed. Each disk was allowed to evolve for 1 My.

As we explained above, we can apply the growth timescale criterion (Section 2.3.4) to the system before the *GAME* calculation is performed. As the *GAME* simulation progresses, we test the remaining four criteria. In particular, we first calculate whether or not any bodies satisfy the mass ratio, mass resolution criteria, and disk eccentricity criteria described in Sections 2.3.1–2.3.3. If any bodies pass these criteria, then we test against the crowded criterion, described in Section 2.3.4. Because of the inside-out nature of growth in the disk, we only consider outward-going migration (that is, the inward-side of any embryo will always fail the crowded criterion).

To test the crowded criterion, we determine if a body is at least $10\times$ more massive than any other body in both its own semimajor axis bin or the bin immediately outward of it. This is somewhat conservative, because, as we showed in Fig. 4, migrating bodies

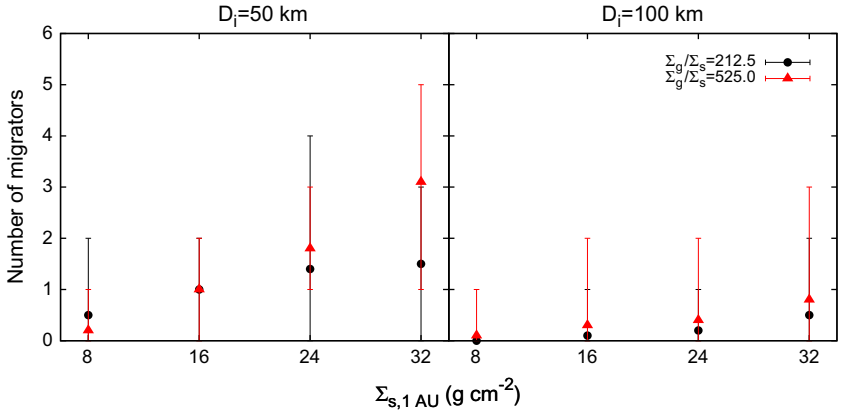

Fig. 11. Average number of objects that satisfy all five migration criteria simultaneously per disk as a function of disk mass ($\Sigma_{s,1AU}$), for different values of initial planetesimal size ($\overline{D}_i$) and gas-to-solid ratio (Σ_g/Σ_s) based on *GAME* results. Initial planetesimal diameters are taken from a normal distribution with dispersion $\sigma_i = \frac{1}{2}\overline{D}_i$. Error bars represent the range of outcomes obtained in *GAME* runs using similar disk criteria.

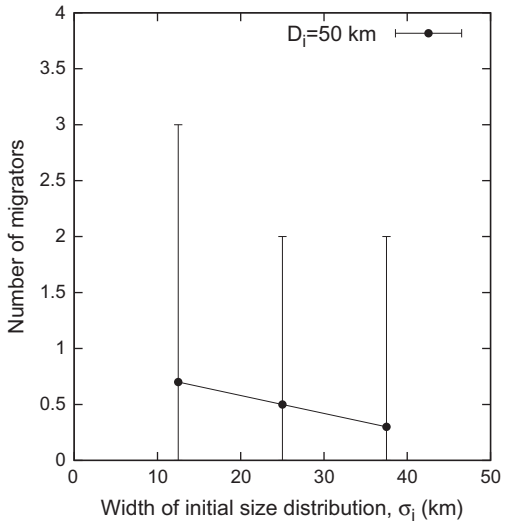

Fig. 12. Average number of objects that satisfy all five migration criteria simultaneously per disk as a function of initial planetesimal dispersion, σ_i. Initial planetesimal diameters are taken from a normal distribution with mean diameter $\overline{D}_i = 50$ km, and disk surface mass density is $\Sigma_s = 8\ \mathrm{g\ cm^{-2}}(r/1\ \mathrm{AU})^{-3/2}$. Error bars represent the range of outcomes obtained in *GAME* runs using similar disk criteria.

only 5× more massive than bodies that they encountered sometimes were able to migrate past.

Fig. 7 shows an example of the disk evolution during a typical *GAME* run. This run is for a 4 × MMSN disk ($\Sigma_{s,1AU} = 32\ \mathrm{g\ cm^{-2}}$ and $p = -1.5$) for planetesimals with an initial mean mass $\overline{D}_i = 100$ km and dispersion of 50 km. The upper panels of Fig. 7 show the mass as a function of semimajor axis for three different times. The lower panels shows the evolution of the disk eccentricity for the same three times. This figure shows how the evolution of the disk is "inside-out," that is that growth of embryos occurs faster in the innermost part of the disk. In general, the disk eccentricity decreases with increasing semimajor axis. The large variations in the inner-most part of the disk result from the fact that large embryos have opened gaps in these regions, and therefore the assumption that the disk eccentricity can be modeled as a distribution with a mean solved by Eq. (19) breaks down.

In Fig. 8 we plot the state of the disk during a typical *GAME* run at the moment that a migration candidate has been identified. The left panel shows the mass of particles in a *GAME* run at a time when a migration candidate has been identified. The migration candidate

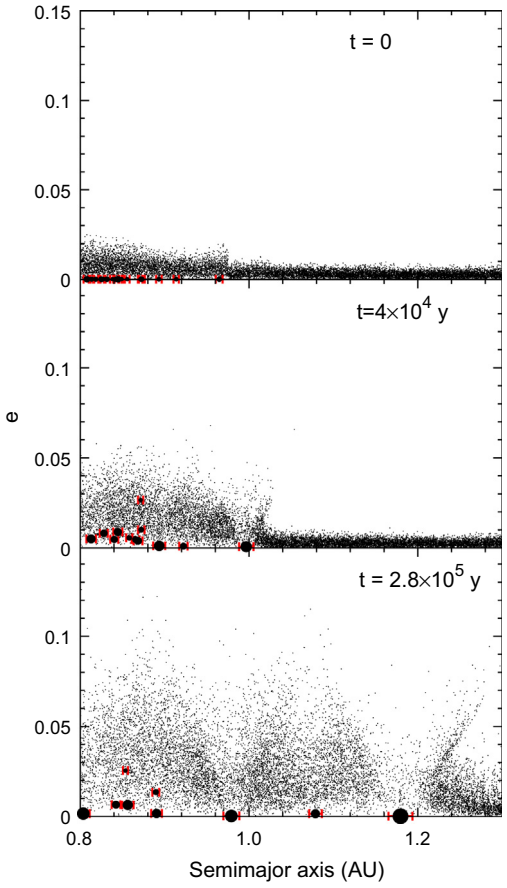

Fig. 13. Snapshots of a versus e for three different times for an N-body SyMBA simulation whose initial conditions were based on a *GAME* run. The *GAME* run was for a $\Sigma_{s,1AU} = 8\ \mathrm{g\ cm^{-2}}$ (1 × MMSN) disk with $\overline{D}_i = 50$ km (this is the same run shown in Fig. 8). The migration candidate emerged at $t = 1.487 \times 10^5$ y at 0.965 AU with a mass of $2.9 \times 10^{-3}\ M_\oplus$. Note that times in the figure are taken from the beginning of the N-body simulation and do not include the 1.487×10^5 y it took for the embryo to form. The large circles are embryos with a size proportional to the embryo radius, and the small circles are the planetesimals. The migration candidate is the outermost embryo. Only 1 of every 5 planetesimals is plotted here. The red error bars span 10× the Hill's radius both inward and outward. (For interpretation of the references to color in this figure legend, the reader is referred to the web version of this article.)

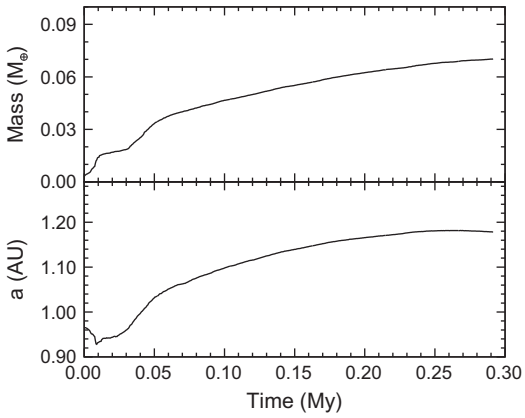

Fig. 14. The semimajor axis and mass versus time of the migration candidate embryo in the simulation shown in Fig. 13. The *GAME* run was for a $\Sigma_{s,1\ AU} = 8$ g cm^{-2} ($1 \times$ MMSN) disk with $\overline{D}_i = 50$ km. The migration candidate emerged at $t = 1.487 \times 10^5$ y at 0.965 AU with a mass of 2.9×10^{-3} M$_\oplus$. Note that times in the figure are taken from the beginning of the N-body simulation and do not include the 1.487×10^5 y it took for the embryo to form. The migration candidate migrated to ~1.2 AU while growing in mass to $\sim 7 \times 10^{-2}$ M$_\oplus$ before halting due to failure of the mass ratio criterion.

is indicated by a star. The right panel illustrates the disk eccentricity criteria by recasting the eccentricity cutoff in terms of mass:

$$M_{\varepsilon,crit} = 3\ \mathrm{M}_\odot (e_{RMS}/\varepsilon_{crit})^3, \tag{18}$$

where ε_{crit} is the critical eccentricity scaled by the Hill factor above which PDM is no longer effective. Embryos with masses above $M_{\varepsilon,crit}$ satisfy the disk eccentricity criterion. The right panel of Fig. 8 plots $M_{\varepsilon,crit}$ as a function of semimajor axis for $\varepsilon_{crit} = 5$. The location migration candidate is indicated as a star on this plot. As $M_{\varepsilon,crit}$ is simply proportional to e^3_{RMS}, this plot shows how the disk eccentricity has evolved in this *GAME* run. Fig. 8 shows a general result of our simulations—if an object even marginally satisfies the disk eccentricity criterion and begins relatively slow outward PDM, it will soon encounter colder disk material and thus be able to migrate at the rate given by Eq. (1).

The results of our parameter study are summarized in Table 1. The table lists the parameters of each type of run (disk mass, gas-to-solids ratio, and mean initial planetesimal diameter) as well as the number of runs with these parameters. All runs in the above *GAME* simulations had $p = -1.5$. In the next columns we list the number of objects that satisfy the crowded criterion alone, and then those that satisfied all five criteria in total for all runs. All migration candidates that satisfied the crowded criterion also satisfied the mass ratio and mass resolution criteria. Some of these objects failed the disk eccentricity criteria, so the total number of objects that satisfied all five criteria is lower than those that only satisfied the crowded criterion.

Fig. 9 shows all objects that satisfy the crowded criterion. However, some of those objects are above the $\varepsilon = 5$ cutoff (dashed line) that defines our disk eccentricity criterion, and therefore are not expected to migrate. The semimajor axis and eccentricity scaled by the Hill factor are plotted at the time that *GAME* identified that they met the crowded criterion. We see little difference between runs with a high gas-to-solid ratio compared to those with a lower ratio (opened and filled circles, respectively). Therefore, the ability of disk to produce objects capable of PDM is not sensitive to the gas-to-solid ratio (at least for the values of $\overline{D}_i$ we have studied here).

Fig. 10 shows the mass versus semimajor axis of all migration candidates (those that satisfy all five PDM criteria). We see that most migration candidates emerge from a narrow zone between ~0.7 and 1.2 AU, with many additional candidates out to the edge of the simulated disk at 2 AU. For objects inward of ~0.7 AU the growth timescale criterion is not met (see Fig. 6), and for objects outward of ~1.5 AU the disk eccentricity criterion is often not met (see Fig. 9). The mass of the migration candidates is also confined to 10^{-3}—10^{-1} M$_\oplus$. On average, more massive disks create more massive migration candidates. The occurrence of a migration candidate may affect how later embryos grow, so in *GAME* runs in which a single disk generates multiple migration candidates, the first occurrence of a candidate is indicated with a filled symbol in Fig. 10. Later occurrences are indicated with open symbols.

The number of migration candidates that emerge in a single disk is correlated with both the initial planetesimal size, $\overline{D}_i$, and the disk mass. Fig. 11 shows the statistical results of multiple *GAME* runs with similar characteristics. Disks with $\Sigma_{s,1AU} = 8$ g cm^{-2}, corresponding to $1 \times$ MMSN, with $\overline{D}_i = 100$ km very rarely produce migration candidates (in 20 runs we found only 1 candidate) within 1 My. Disks with $\Sigma_{s,1AU} = 32$ g cm^{-2}, corresponding to $4 \times$ MMSN, with $\overline{D}_i = 50$ km, on the other hand, usually produces several migration candidates within 1 My. Therefore, massive disks with small planetesimals favor PDM of embryos. Recall that the memory limitations of *GAME* require us to keep $\overline{D}_i > 50$ km. And yet it is possible that the initial sizes of planetesimals were much smaller than this (Weidenschilling, 2011), and we may be underestimating the number of embryos capable of experiencing PDM. We have also separated out runs with different values of the gas-to-solid ratio (Σ_g/Σ_s). There appears to be a slight bias toward more migration candidates for the more gas-rich disk, but only one set of conditions ($\Sigma_{s,1AU} = 32$ g cm^{-2}, $D_i = 50$ km) produced a significant difference.

We also explored the effect that the shape of the initial size distribution of the planetesimals has on the number of migration candidates. Because we took our initial size distribution from a Gaussian distribution, the width of the distribution (given by the variance, σ_i^2) was a free parameter. We performed a repeat of the *GAME* runs with $\Sigma_{s,1AU} = 8$ g cm^{-2} and $\overline{D}_i = 50$ km, but varied the width of the initial distribution, σ_i to be $\frac{1}{4}, \frac{1}{2}$, and $\frac{3}{4}\overline{D}_i$. The results are shown in Fig. 12. The average number of migration candidates was slightly higher for disks with the narrower initial size distribution, but it is not clear that this is significant given the small total numbers of candidates in each simulation.

4. Conclusion and discussion

Planetesimal-driven migration (PDM) is potentially an important process in the evolution of the inner Solar System. In particular, the effects of PDM may alter the mass and semimajor axis distribution of embryos during the early stages of planet formation. In the standard model for terrestrial planet formation, embryos form in the runaway and oligarchic growth stages until they deplete their local feeding zones. Planets then form in the late-accretion stage as a consequence of embryo–embryo mergers. We show that some embryos may not remain stationary, but instead may migrate outward.

We have identified five criteria that must be met in order for any particular embryo within a planetesimal disk to begin planetesimal-driven migration. These criteria are detailed in Sections 2.3.1–2.3.5, and are summarized as follows: (1) The mass ratio criterion (Section 2.3.1): A migrating embryo must be at least $3\times$ more massive than the total mass of planetesimals in its encounter zone. (2) The mass resolution criterion (Section 2.3.2): A migrating embryo must be at least $100\times$ more massive than the average planetesimal it encounters. (3) The disk eccentricity criterion (Section 2.3.3): The local eccentricity scaled by the Hill factor, defined in Eq. (5), of the planetesimal disk that a migrating embryo is

embedded in must be less than 5. (4) The crowded criterion (Section 2.3.4): A migrating embryo must be 5–10× more massive than any body that it encounters. (5) The growth timescale criterion (Section 2.3.5): A migrating embryo must outpace the outwardly propagating embryo formation front within the disk. For a variety of plausible Solar System planetesimal disks, we find that only embryos that form outward of ~0.7–1.0 AU satisfy the growth timescale criterion.

Using a Monte Carlo code we have developed called *GAME*, we model the growth of embryos from a planetesimal disk in order to determine which Solar System-like disks produce embryos that satisfy all five of the above PDM criteria. *GAME* models embryo formation through pairwise merging of discrete bodies in such a way that approximates analytical models of runaway and oligarchic growth. Through *GAME* simulations we have determined that Solar System-like disks produce on the order a few embryos capable of undergoing PDM in the terrestrial planet formation zone between ~0.7 and 2.0 AU. The number of migrating embryos produced by any given disk is correlated with disk mass, that is, more massive disks produce more migrating bodies on average than less massive disks. In disks with $\Sigma_{s,1\mathrm{AU}} = 8\ \mathrm{g\ cm^2}$ (the standard minimum mass solar nebula disk), in 40 runs we produced an average of 0.2 migrating embryos per run. Only one simulation out of the 40 produced 2 candidates. The rest produced 0 or 1. In contrast, out of 40 runs with disks 4× as massive, we produced an average of 1.5 migrating embryos per run. One simulation out of the 40 produced 7 candidates. The number of migrating embryos is also correlated with the initial mass of the planetesimals, such that disks with smaller planetesimals tend to produce more migrating embryos on average than disks with larger planetesimals. In simulations with $\Sigma_{s,1\mathrm{AU}} = 8\ \mathrm{g\ cm^2}$ and $\overline{D}_i = 50$ km, we produced an average of 0.4 migration candidates per simulation, but with $\overline{D}_i = 100$ km we only produced 0.05 candidates on average. For 4× more massive disks, we produced an average of 2.3 and 0.7 migration candidates for $\overline{D}_i = 50$ km and 100 km, respectively, and all but one disk with $\overline{D}_i = 50$ km produced at least one PDM candidate. Due to memory limitations of the *GAME* code, we have only simulated disks with initial planetesimals of $\overline{D}_i = 50$—100 km. We find no correlation between the number of migrating embryos produced by a disk and the solid to gas ratio of the disk.

In our analysis, we have assumed that turbulence is not important for the eccentricity distribution of planetesimals. It has been shown that density variations in the gas disk due to turbulence may excite planetesimal eccentricities (Ogihara et al., 2007; Ida et al., 2008; Yang et al., 2009; Nelson and Gressel, 2010; Gressel et al., 2011; Yang et al., 2012). Ida et al. (2008) suggested that the eccentricity excitation due to turbulence should be so high at 1 AU that collisions between planetesimals with $D < 300$ km would always be erosive. This level of eccentricity excitation would likely preclude PDM of any embryos due to failure of the disk eccentricity criterion (Section 2.3.3). However, the amount of eccentricity excitation in that model was a function of a dimensionless hydrodynamic turbulence strength parameter, γ. Yang et al. (2009) using a different disk model produced an equivalent value of γ that was a factor of ~5 less than the fiducial value of Ida et al. (2008), and concluded that turbulence was not an important factor in setting planetesimal eccentricity. As evaluating models of disk turbulence is beyond the scope of the present work, we did not consider the effect of turbulence.

Here we determine how the migration process might effect the growth of planets in the 1–1.5 AU region. We accomplish this with a direct N-body simulation. We took a snapshot of a *GAME* simulation at the moment a migration candidate was identified to generate a set of initial conditions for an N-body simulation, which was done with SyMBA. This run was for a $\Sigma_{s,1\mathrm{AU}} = 8\ \mathrm{g\ cm^{-2}}$ and $p = -1.5$ ($1 \times$ MMSN) disk with $\overline{D}_i = 50$ km. The migration candidate emerged at $t = 1.487 \times 10^5$ y at 0.965 AU with a mass of $2.9 \times 10^{-3}\ \mathrm{M_\oplus}$ (about a quarter of a lunar mass). At this point in time, there were $\sim 5 \times 10^6$ particles remaining in the *GAME* simulation—many more than can be handled in a N-body simulation. Thus, we employed the following algorithm for generating the initial conditions for the disk particles.

In Section 2.3.2 we showed that if the masses of individual disk particles were within a factor of ~100 the mass of the embryo then they can affect migration, but the embryo's behavior was insensitive to the mass of the individual planetesimals if they were smaller than this. Thus, in order to preserve the graininess of the disk, we kept all the larger planetesimals. In particular, in order to be conservative, if the masses of any particular *GAME* particle were greater than 1/200 the mass of the migration candidate, that particle was retained as an individual body in the SyMBA simulation. The rest of the particles were combined into particles with 1/200 the mass of the migration candidate, in such a way that the mass versus semimajor axis distribution mimicked that of the full set of small *GAME* particles. The e and i of these small particles were drawn from Rayleigh distributions with a mean based on values from the *GAME* snapshot.

In order to reduce the amount of integration time, we only used the portion of the *GAME* disk between 0.8 and 2.0 AU. Particles with mass greater than 0.5× the mass of the migration candidate were considered "embryos" and fully interacted gravitationally with each other. Particles less than this mass were considered "planetesimals" and gravitationally affected the embryos, but not each other. This procedure resulted in a SyMBA input file with ~144,000 particles, 20 of which were fully interacting embryos. Choosing to limit the mass cutoff to 0.5× the mass of the migration candidate was done so for expediency. The total integration time using the parallelized SyMBA took approximately three months. We estimate that, had we chosen a mass cutoff of 0.2× the mass of the migration candidate, the same simulation would have taken 2 years. The surface mass density, eccentricity, and inclination as a function of semimajor axis of the planetesimals of the SyMBA initial conditions matched as closely as possible that described by the *GAME* snapshot at the moment of the migration candidate emergence.

The global integration stepsize for the SyMBA integration was set to 0.02 y, and the integration was halted after 2.9×10^5 y. No nebular gas effects were simulated. Three snapshots of a versus e for the initial conditions, $t = 4 \times 10^4$ y, and the final time are shown in Fig. 13. (Note that times in the figure are taken from the beginning of the N-body simulation and do not include the 1.487×10^5 y it took for the embryo to form.) These snapshots show the general behavior of the system is consistent with that expected. The migration candidate migrate away from the region it emerges from. The mass and semimajor axis as a function of time for the migration candidate in the SyMBA run are plotted in Fig. 14. We see that the candidate initially migrates inwards, but encounters a similar-sized embryo and scatters away from it, and thus reverses direction. In other words, the migration candidate fails the crowded criterion for inward-going PDM. However, no similar-sized embryos exist in the outward-going direction, so the migration candidate migrates outward unhindered. Migration slows down and ultimately halts when the migrating embryo reaches ~1.2 AU. At this point it has grown to a mass of $\sim 0.07\ \mathrm{M_\oplus}$, and migration halts because it fails the mass ratio criterion for value for $\Sigma_{s,1\mathrm{AU}}$ (see Eq. (7) and Fig. 2).

The behavior of the above simulation is consistent with that expected based on our discussion of the role of PDM so far, and the final distribution of embryos shown in the bottom panel of Fig. 13 is very different than the standard distribution used as initial conditions for in late-stage accretion simulations. To illustrate

this, we plotted each embryo in Fig. 13 with red error bars that are drawn to span $10 \times R_H$ both inward and outward, which is the assumed characteristic spacing of embryos at the start of late stage accretion (Kokubo and Ida, 1998). The outermost embryos (the ones that have experienced PDM) are spaced many 10s of R_H apart from each other. PDM may therefore be an important part of the formation history of planets, and it should not be ignored.

Acknowledgments

We would like to thank Alessandro Morbidelli and two anonymous reviewers for their helpful comments. The work also greatly benefited from discussions and input from William Bottke, Scott Kenyon, and Ben Bromley. This work was funded through a grant from NASA Lunar Science Institute (NNA09DB32A, PI: William F. Bottke).

Appendix A. Description of the Monte Carlo planetesimal merger code *GAME*

GAME (Growth And Migration of Embryos) uses a Monte Carlo approach to simulate the growth of planetesimals into planetary embryos, described by Eq. (11) for a population of planetesimals with a realistic initial masses. There are two components to *GAME*: individual bodies, and binned disk parameters. The individual bodies are stored in array, and each element contains information about the body's mass, diameter, and semimajor axis. The disk component is stored in a smaller array that represents average properties of the disk within finite semimajor axis bins. Each element of the disk properties array contains the inner and outer boundary of the bin, the mean eccentricity and inclination, the median planetesimal mass, the total mass and number of oligarchs, the surface mass density of oligarchs, and the total surface mass density of the bin. Objects are considered to be oligarchs if their mass is greater than the planetesimal-to-oligarch transition mass defined by Eq. (10).

First, a population of planetesimals is constructed with some surface mass density, $\Sigma_m(a)$, using i particles drawn from a mass distribution set by the user. Each particle represents a single planetesimal in the disk. The initial eccentricity of the disk is set by the user, and disk properties are computed in every bin based on the population of bodies found within.

In a time interval Δt we solve for the mass growth ΔM_i based on Eq. (11), and using disk properties from the bin where particle i resides. Then we randomly select particle j out of a population of nearby particles (we use $5\times$ the Hill's radii as the size of the feeding zone for this work). Gravitational focusing is implicitly included in Eq. (11).

Once particle j is chosen, we then choose a random number p_{merge} from a uniform distribution between 0 and 1. If $p_{merge} < \Delta M_i/Mj$, then a merger takes place and the mass of particle j is added to that of particle i, and particle j is taken out of existence. The semimajor axis of particle i is updated with the mass-weighted mean of the semimajor axes of i and j. If $\Delta M_i/Mj > 1$, then the above procedure is repeated with $\Delta M_i' \rightarrow \Delta M_i - M_j$. If $p_{merge} > \Delta M_i/Mj$, then no merger takes place, but the particle is given a change in semimajor axis (in a random direction) to approximate effects of close encounters. We do this using the semimajor axis drift rate for particles experiencing PDM given by Eq. (1).

Once the merger calculation is finished, then i is iterated to the next object, and the procedure is repeated until all objects have been sampled. The binned disk properties are then recalculated using the updated state of the particle disk. The eccentricity of the disk is calculated using an adaptive stepsize Runge–Kutta algorithm to solve:

$$\frac{de^2}{dt} = \frac{e^2}{T_{VS}} - \frac{e^2}{T_{gas}}, \tag{19}$$

where T_{VS} is one of the viscous stirring timescales, either Eq. (13) or (14) based on whether or not oligarchs are present within the bin, and T_{gas} is the gas damping timescale given by Eq. (15). The inclination is set to half the eccentricity.

GAME also contains a simple fragmentation model. The relative velocity at the time of merger is estimated using the relationships estimated by Lissauer and Stewart (1993), where:

$$v_{imp} = \left(\frac{5}{4}e^2 + i^2\right)^{1/2}. \tag{20}$$

Using the strength law of Benz and Asphaug (1999), we calculate a fragmentation parameter, p_{frag}, where:

$$p_{frag} = \frac{v_{imp}^2}{2Q_D^*}, \tag{21}$$

and Q_D^* is the specific energy required to remove half the mass of the body. If $p_{frag} > 1$, then the merger is not allowed to proceed, even if $p_{merge} < \Delta M_i/Mj$.

The approach of *GAME* has significant advantages to the problem of identifying migration candidates over statistical codes such as *Boulder* (cf., Morbidelli et al., 2009). Because of the crowded criterion, described in Section 2.3.4, objects that are candidates for planetesimal-driven migration must be at least 5–10× more massive than any of its nearby neighbors. Therefore that body is by definition a statistical outlier in the local mass distribution.

References

Adachi, I., Hayashi, C., Nakazawa, K., 1976. The gas drag effect on the elliptical motion of a solid body in the primordial solar nebula. Prog. Theor. Phys. 56, 1756–1771.
Agnor, C.B., Canup, R.M., Levison, H.F., 1999. On the character and consequences of large impacts in the late stage of terrestrial planet formation. Icarus 142 (1), 219–237.
Andrews, S.M., Wilner, D.J., Hughes, A.M., Qi, C., Dullemond, C.P., 2010. Protoplanetary disk structures in Ophiuchus. II. Extension to fainter sources. Astrophys. J. 723, 1241–1254.
Armitage, P.J., 2007. Lecture notes on the formation and early evolution of planetary systems. arXiv astro-ph.
Armitage, P.J., 2010. Dynamics of protoplanetary disks. arXiv astro-ph.SR.
Batygin, K., Brown, M.E., 2010. Early dynamical evolution of the Solar System: Pinning down the initial conditions of the nice model. Astrophys. J. 716 (2), 1323–1331.
Benz, W., Asphaug, E., 1999. Catastrophic disruptions revisited. Icarus 142, 5–20.
Brasser, R., 2013. The formation of Mars: Building blocks and accretion time scale. Space Sci. Rev. 174 (1), 11–25.
Bromley, B.C., Kenyon, S.J., 2006. A hybrid n-body-coagulation code for planet formation. Astron. J. 131, 2737–2748.
Bromley, B.C., Kenyon, S.J., 2011. Migration of planets embedded in a circumstellar disk. Astrophys. J. 735 (1), 29–43.
Bryden, G., Lin, D.N.C., Ida, S., 2000. Protoplanetary formation. I. Neptune. Astrophys. J. 544 (1), 481–495.
Capobianco, C.C., Duncan, M., Levison, H.F., 2011. Planetesimal-driven planet migration in the presence of a gas disk. Icarus 211, 819–831.
Chambers, J.E., 2001. Making more terrestrial planets. Icarus 152 (2), 205–224.
Chambers, J.E., Wetherill, G.W., 1998. Making the terrestrial planets: N-body integrations of planetary embryos in three dimensions. Icarus 136, 304–327.
Chiang, E., Youdin, A.N., 2010. Forming planetesimals in solar and extrasolar nebulae. Ann. Rev. Earth Planet. Sci. 38, 493–522.
Duncan, M.J., Levison, H.F., Lee, M.H., 1998. A multiple time step symplectic algorithm for integrating close encounters. Astron. J. 116, 2067–2077.
Fernandez, J.A., Ip, W.-H., 1984. Some dynamical aspects of the accretion of Uranus and Neptune – The exchange of orbital angular momentum with planetesimals. Icarus 58, 109–120.
Fraser, W.C., Kavelaars, J.J., Holman, M.J., Pritchet, C.J., Gladman, B.J., Grav, T., Jones, R.L., Macwilliams, J., Petit, J.-M., 2008. The Kuiper belt luminosity function from $m = 21$ to 26. Icarus 195 (2), 827–843.
Gomes, R., Levison, H.F., Tsiganis, K., Morbidelli, A., 2005. Origin of the cataclysmic late heavy bombardment period of the terrestrial planets. Nature 435 (7), 466–469.
Greenberg, R., Hartmann, W.K., Chapman, C.R., Wacker, J.F., 1978. Planetesimals to planets – Numerical simulation of collisional evolution. Icarus 35, 1–26.

Gressel, O., Nelson, R.P., Turner, N.J., 2011. On the dynamics of planetesimals embedded in turbulent protoplanetary discs with dead zones. Mon. Not. R. Astron. Soc. 415 (4), 3291–3307.
Hayashi, C., 1981. Structure of the solar Nebula, Growth and decay of magnetic fields and effects of magnetic and turbulent viscosities on the Nebula. Prog. Theoret. Phys. Suppl. 70, 35–53.
Hubickyj, O., Bodenheimer, P., Lissauer, J.J., 2005. Accretion of the gaseous envelope of Jupiter around a 5 10 Earth-mass core. Icarus 179, 415–431.
Ida, S., Makino, J., 1992. N-body simulation of gravitational interaction between planetesimals and a protoplanet. I – Velocity distribution of planetesimals. Icarus 96, 107–120.
Ida, S., Makino, J., 1993. Scattering of planetesimals by a protoplanet – Slowing down of runaway growth. Icarus 106, 210–227.
Ida, S., Bryden, G., Lin, D.N.C., Tanaka, H., 2000. Orbital migration of Neptune and orbital distribution of trans-Neptunian objects. Astrophys. J. 534, 428–445.
Ida, S., Guillot, T., Morbidelli, A., 2008. Accretion and destruction of planetesimals in turbulent disks. Astrophys. J. 686 (2), 1292–1301.
Kenyon, S.J., Bromley, B.C., 2006. Terrestrial planet formation. I. The transition from oligarchic growth to chaotic growth. Astron. J. 131 (3), 1837–1850.
Kirsh, D.R., Duncan, M., Brasser, R., Levison, H.F., 2009. Simulations of planet migration driven by planetesimal scattering. Icarus 199 (1), 197–209.
Kokubo, E., Ida, S., 1995. Orbital evolution of protoplanets embedded in a swarm of planetesimals. Icarus 114, 247–257.
Kokubo, E., Ida, S., 1996. On runaway growth of planetesimals. Icarus 123, 180–191.
Kokubo, E., Ida, S., 1998. Oligarchic growth of protoplanets. Icarus 131, 171–178.
Kokubo, E., Ida, S., 2000. Formation of protoplanets from planetesimals in the solar Nebula. Icarus 143, 15–27.
Kokubo, E., Ida, S., 2002. Formation of protoplanet systems and diversity of planetary systems. Astrophys. J. 581, 666–680.
Kominami, J., Ida, S., 2002. The effect of tidal interaction with a gas disk on formation of terrestrial planets. Icarus 157 (1), 43–56.
Leinhardt, Z.M., Richardson, D.C., 2005. Planetesimals to protoplanets. I. Effect of fragmentation on terrestrial planet formation. Astrophys. J. 625 (1), 427–440.
Leinhardt, Z.M., Richardson, D.C., Lufkin, G., Haseltine, J., 2009. Planetesimals to protoplanets – II. Effect of debris on terrestrial planet formation. Mon. Not. R. Astron. Soc. 396 (2), 718–728.
Levison, H.F., Morbidelli, A., Gomes, R., Backman, D., 2007. Planet migration in planetesimal disks. Protostars Planets V, 669–684.
Levison, H.F., Thommes, E., Duncan, M.J., 2010. Modeling the formation of giant planet cores. I. Evaluating key processes. Astron. J. 139, 1297–1314.
Lissauer, J.J., 1987. Timescales for planetary accretion and the structure of the protoplanetary disk. Icarus 69 (2), 249–265.
Lissauer, J.J., Stewart, G.R., 1993. Growth of planets from planetesimals. Protostars Planets III -1, 1061–1088.
Malhotra, R., 1993. The origin of Pluto's peculiar orbit. Nature 365, 819–821.
Mizuno, H., Nakazawa, K., Hayashi, C., 1978. Instability of a gaseous envelope surrounding a planetary core and formation of giant planets. Prog. Theor. Phys. 60, 699–710.
Morbidelli, A., Levison, H.F., Tsiganis, K., Gomes, R., 2005. Chaotic capture of Jupiter's Trojan asteroids in the early Solar System. Nature 435 (7), 462–465.
Morbidelli, A., Bottke, W.F., Nesvorný, D., Levison, H.F., 2009. Asteroids were born big. Icarus 204 (2), 558–573.
Morishima, R., Stadel, J., Moore, B., 2010. From planetesimals to terrestrial planets: N-body simulations including the effects of nebular gas and giant planets. Icarus 207, 517–535.
Nagasawa, M., Lin, D.N.C., Thommes, E., 2005. Dynamical shake-up of planetary systems. I. Embryo trapping and induced collisions by the sweeping secular resonance and embryo-disk tidal interaction. Astrophys. J. 635 (1), 578–598.
Nelson, R.P., Gressel, O., 2010. On the dynamics of planetesimals embedded in turbulent protoplanetary discs. Mon. Not. R. Astron. Soc. 409 (2), 639–661.
Nesvorný, D., Morbidelli, A., 2012. Statistical study of the early Solar System's instability with four, five, and six giant planets. Astron. J. 144 (4), 117–136.
Nesvorný, D., Youdin, A.N., Richardson, D.C., 2010. Formation of Kuiper belt binaries by gravitational collapse. Astron. Journal 140, 785–793.
O'Brien, D.P., Morbidelli, A., Levison, H.F., 2006. Terrestrial planet formation with strong dynamical friction. Icarus 184 (1), 39–58.
Ogihara, M., Ida, S., Morbidelli, A., 2007. Accretion of terrestrial planets from oligarchs in a turbulent disk. Deep Impact Mission Comet 9P/Tempel Part 1 188 (2), 522–534.
Pollack, J.B., Hubickyj, O., Bodenheimer, P., Lissauer, J.J., Podolak, M., Greenzweig, Y., 1996. Formation of the Giant planets by concurrent accretion of solids and gas. Icarus 124, 62–85.
Raymond, S.N., Quinn, T., Lunine, J.I., 2005. Terrestrial planet formation in disks with varying surface density profiles. Astrophys. J. 632, 670–676.
Raymond, S.N., Quinn, T., Lunine, J.I., 2006. High-resolution simulations of the final assembly of Earth-like planets I. Terrestrial accretion and dynamics. Icarus 183, 265–282.
Raymond, S.N., O'Brien, D.P., Morbidelli, A., Kaib, N.A., 2009. Building the terrestrial planets: Constrained accretion in the inner Solar System. Icarus 203 (2), 644–662.
Safronov, V.S., 1972. Evolution of the protoplanetary cloud and formation of the Earth and planets.
Spaute, D., Weidenschilling, S.J., Davis, D.R., Marzari, F., 1991. Accretional evolution of a planetesimal swarm. I – A new simulation. Icarus 92, 147–164.
Thommes, E.W., Duncan, M.J., Levison, H.F., 2003. Oligarchic growth of giant planets. Icarus 161, 431–455.
Tsiganis, K., Gomes, R., Morbidelli, A., Levison, H.F., 2005. Origin of the orbital architecture of the giant planets of the Solar System. Nature 435 (7), 459–461.
Weidenschilling, S.J., 1977a. Aerodynamics of solid bodies in the solar nebula. R. Astron. Soc. 180, 57–70.
Weidenschilling, S.J., 1977b. The distribution of mass in the planetary system and solar nebula. Astrophys. Space Sci. 51, 153–158.
Weidenschilling, S.J., 1980. Dust to planetesimals – Settling and coagulation in the solar nebula. Icarus 44, 172–189.
Weidenschilling, S.J., 2011. Initial sizes of planetesimals and accretion of the asteroids. Icarus 214 (2), 671–684.
Weidenschilling, S.J., Spaute, D., Davis, D.R., Marzari, F., Ohtsuki, K., 1997. Accretional evolution of a planetesimal swarm. Icarus 128, 429–455.
Wetherill, G.W., 1980. Formation of the Terrestrial Planets. Ann. Rev. Astron. Astrophys. 18 (1), 77–113.
Wetherill, G.W., 1985. Occurrence of giant impacts during the growth of the terrestrial planets. Science 228 (4701), 877–879.
Wetherill, G.W., 1990. Formation of the Earth. Ann. Rev. Earth Planet. Sci. 18 (1), 205–256.
Wetherill, G.W., 1991. Why Isn't Mars as Big as Earth? Lunar Planet. Sci. Conf. Abstracts 22, 1495–1496.
Wetherill, G.W., 1992. An alternative model for the formation of the asteroids. Icarus 100, 307–325.
Wetherill, G.W., Stewart, G.R., 1989. Accumulation of a swarm of small planetesimals. Icarus 77, 330–357.
Wetherill, G.W., Stewart, G.R., 1993. Formation of planetary embryos – Effects of fragmentation, low relative velocity, and independent variation of eccentricity and inclination. Icarus 106, 190–209.
Yang, C.-C., Mac Low, M.-M., Menou, K., 2009. Planetesimal and protoplanet dynamics in a turbulent protoplanetary disk: Ideal unstratified disks. Astrophys. J. 707 (2), 1233–1246.
Yang, C.-C., Mac Low, M.-M., Menou, K., 2012. Planetesimal and protoplanet dynamics in a turbulent protoplanetary disk: Ideal stratified disks. Astrophys. J. 748 (2), 79–94.